Geomorphology 221 (2014) 298–319

Contents lists available at ScienceDirect

Geomorphology

journal homepage: www.elsevier.com/locate/geomorph

Semi-automated mapping of landforms using multiple point geostatistics

E. Vannametee *, L.V. Babel, M.R. Hendriks, J. Schuur, S.M. de Jong, M.F.P. Bierkens, D. Karssenberg

Department of Physical Geography, Faculty of Geosciences, Utrecht University, PO Box 80115, 3508 TC Utrecht, The Netherlands

ARTICLE INFO

Article history:
Received 1 October 2013
Received in revised form 30 May 2014
Accepted 31 May 2014
Available online 18 June 2014

Keywords:
Automated landform mapping
Landscape delineation
Multiple point geostatistics
SNESIM
Buëch
French Alps

ABSTRACT

This study presents an application of a multiple point geostatistics (MPS) to map landforms. MPS uses information at multiple cell locations including morphometric attributes at a target mapping cell, i.e. digital elevation model (DEM) derivatives, and non-morphometric attributes, i.e. landforms at the neighboring cells, to determine the landform. The technique requires a training data set, consisting of a field map of landforms and a DEM. Mapping landforms proceeds in two main steps. First, the number of cells per landform class, associated with a set of observed attributes discretized into classes (e.g. slope class), is retrieved from the training image and stored in a frequency tree, which is a hierarchical database. Second, the algorithm visits the non-mapped cells and assigns to these a realization of a landform class, based on the probability function of landforms conditioned to the observed attributes as retrieved from the frequency tree. The approach was tested using a data set for the Buëch catchment in the French Alps. We used four morphometric attributes extracted from a 37.5-m resolution DEM as well as two non-morphometric attributes observed in the neighborhood. The training data set was taken from multiple locations, covering 10% of the total area. The mapping was performed in a stochastic framework, in which 35 map realizations were generated and used to derive the probabilistic map of landforms. Based on this configuration, the technique yielded a map with 51.2% of correct cells, evaluated against the field map of landforms. The mapping accuracy is relatively high at high elevations, compared to the mid-slope and low-lying areas. *Debris slope* was mapped with the highest accuracy, while MPS shows a low capability in mapping *hogback* and *glacis*. The mapping accuracy is highest for training areas with a size of 7.5–10% of the total area. Reducing the size of the training images resulted in a decreased mapping quality, as the frequency database only represents local characteristics of landforms that are not representative for the remaining area. MPS outperforms a rule-based technique that only uses the morphometric attributes at the target mapping cell in the classification (i.e. one-point statistics technique), by 15% of cell accuracy.

1. Introduction

Geomorphological maps are among the most important tools for studying earth surface processes. Field maps of landforms, in combination with other terrestrial archives such as aerial photographs and satellite images, can deliver useful information for land evaluation, landscape planning, geo-hazard risk assessment, and analysis of landscape evolution (e.g. Otto and Dikau, 2004). Manual derivation of landform maps is labor-intensive and time-consuming, particularly for large areas (Adediran et al., 2004). Mapping quality may be influenced by individual experiences in landscape interpretation, which can result in bias in landform categorization (Williams et al., 2012). These problems encourage scientists to resort to automated landform mapping, because the amount of fieldwork can be largely reduced (Seijmonsbergen et al., 2011). Automated mapping is particularly useful for areas with limited accessibility, such as high and dense-forested regions (e.g. Schneevoigt et al., 2008) and planetary surfaces other than those on the Earth (Florinsky, 2008), i.e. Mars (e.g. Stepinski et al., 2007), Venus (e.g. Burl et al., 1994), and the Moon (e.g. Jain et al., 2013).

Automated landform classification has shown a rapid growth over recent years due to advances in machine-learning technologies and the increasing availability of high-resolution digital terrain data (Evans, 2012). Automated landform classification can be done following inductive or deductive approaches, or a combination of these. The inductive approach, also referred to as unsupervised classification, derives landform classes based on internal characteristics and self-organizing structure of the terrain attributes without imposing prior knowledge of the geomorphological characteristics (Irvin et al., 1997; Burrough et al., 2000; Bue and Stepinski, 2006; Etzelmüller et al., 2007). The deductive approach performs the classification based on pre-set class definitions of the cell properties representing particular landform classes obtained from field evidence, i.e. supervised classification (Hengl and Rossiter, 2003; Reuter et al., 2006; Seijmonsbergen, 2008; Ho et al., 2013). Digital elevation models (DEMs) are primarily used to deliver morphometric attributes such as slope for identifying different landform types (Sulebak et al., 1997; Bolongaro-Crevenna et al., 2005; Gharari et al., 2011). Non-morphometric information related to vegetation, lithology,

* Corresponding author. Tel.: +31 302532183.
E-mail address: e.vannametee@uu.nl (E. Vannametee).

http://dx.doi.org/10.1016/j.geomorph.2014.05.032
0169-555X/

land cover, and soil derived from remote sensing and field observations can be used to improve the classification (Irvin et al., 1997; Benger, 2003; Adediran et al., 2004; Luoto and Hjort, 2005; Schneevoigt et al., 2008; Chartin et al., 2011).

Many existing automated classification techniques delimit landform units based on the statistical analysis of terrain attributes obtained at a single location, often neglecting spatial relations of landscape characteristics and landform patterns. These include, for instance, techniques based on automated data grouping such as clustering (MacMillan et al., 2000), classification trees (Thuiller et al., 2003; Stepinski and Vilalta, 2005; Chartin et al., 2011), and regression (Atkinson et al., 1998; Luoto and Hjort, 2005; Ridefelt et al., 2010). These techniques often produce units lacking spatial coherence, because spatial relations are not considered in the classification (Minár and Evans, 2008). Also, they may result in misrepresentation of morphological breaks (sharp transitions) in the landscape, as this requires information at more than one location to locate terrain discontinuities (van Niekerk, 2010). To overcome this problem, a number of techniques have been proposed that incorporate spatial information and relations between locations. These include region growing approaches (Romstad, 2001; van Asselen and Seijmonsbergen, 2006), terrain segmentation approaches (Dymond et al., 1995; Klingseisen et al., 2008; Matsuura and Aniya, 2012), and approaches using variograms (Jordan, 2003; Bishop et al., 2012) to give information on the spatial continuity of different morphological features that can aid landform discrimination (e.g. Trevisani et al., 2009). These techniques are, however, only based on statistics calculated between two locations, which are often insufficient to capture complex spatial patterns (Wood, 1996; Caers and Zhang, 2004). Applications of the two-point statistics classification techniques are, thus, mainly limited to extracting morphological features that have a relatively simple geometry (e.g. Dymond et al., 1995; Etzelmüller et al., 2007; van Niekerk, 2010), or as a basis for object-based classification (Drăguţ and Blaschke, 2006; Anders et al., 2011).

Multiple point geostatistics (MPS) is developed to overcome limitations of one or two point statistics in simulating complex spatial patterns (Guardiano and Srivastava, 1993). This method characterizes and simulates a random variable at specific locations based on the spatial configuration of properties and their autocorrelations at multiple spatial locations retrieved from a training image (Strebelle, 2002; Caers and Zhang, 2004; de Vries et al., 2009). This training image can be a conceptual drawing, geological analogue, outputs from process-based modeling, or unconditional object-based simulations that contain data patterns deemed present in the area that has to be mapped (Hu and Chugunova, 2008; Honarkhah, 2011). Simulation of a random variable can be done for a 2D domain or image (Liu and Journel, 2004), a 3D block (Comunian et al., 2011), or even in 4D (Wu, 2007). MPS has been widely used to simulate geological facies distribution for petroleum reservoir modeling (Caers, 2001; Strebelle, 2002; Caers and Zhang, 2004), and to reconstruct fluvial depositional architecture for simulation of groundwater and hydrogeological transport (Feyen and Caers, 2005; Knudby and Carrera, 2005; Huysmans and Dassargues, 2009). Recent research applies MPS for mapping the spatial pattern of land surface phenomena; for example, soil type distribution (Meerschman et al., 2013), geological features using outcrop information from LiDAR images (Viseur, 2013), sub-pixel land cover mapping (Boucher, 2007), and rain clusters within cloudy regions (Wojcik et al., 2009). However, to our best knowledge, there has been no attempt to use MPS for mapping landforms.

In this paper, we explore and investigate the use of MPS for landform classification, focusing on medium-scale landform types with a dimension between 10^{-2} and 10^{1} km^2, such as alluvial fans, fluvial terraces, and debris slopes (Dramis et al., 2011). Here, we follow the SNESIM approach (Strebelle, 2002), which is the first practical MPS algorithm that has shown a profound success in many applications (e.g. Feyen and Caers, 2005; Rezaee et al., 2011; Tang et al., 2013). SNESIM retrieves, for each pixel on a training image consisting of a field map of landforms and a DEM, a landform class including associated DEM attributes in categorical values (e.g. slope classes) and landforms at the neighboring pixels. Frequencies (i.e. number of cells) of each landform class corresponding to all sets of attributes observed in the training image are stored in a search tree (i.e. frequency database). In the classification stage, the algorithm stochastically assigns to every pixel, in a sequential order, a realization of a landform class drawn from a conditional probability distribution of landform types, read from the search tree, for observed DEM attributes at the target pixel and previously-mapped landforms in its neighborhood. In this manner, landform mapping can be set in a probabilistic framework using a Monte Carlo simulation approach, giving information on mapping uncertainty. Furthermore, with a capability of using information at multiple cell locations, landforms in the surroundings can be explicitly used to determine the landform class of the target cell. This information is potentially useful in mapping, because landforms exhibit a structural pattern in the landscape due to the dominant geomorphic processes at different locations (Evans and Cox, 1999; Dehn et al., 2001).

As a pioneer study, we will investigate the configuration and implementation of MPS in geomorphological mapping with an aim to answer four questions: 1) What are the key attributes and their associated class discretization that enable the best discrimination between different landforms? 2) What is the capability of the MPS technique in mapping landforms in the study area? 3) What is the relation between size of the training area and mapping quality? 4) What is the performance of MPS relative to a standard classification technique? This study is carried out using a data set from the Buëch region in the French Prealps. To investigate the fourth research question, we use a rule-based approach because it has been widely applied in a stand-alone mode (e.g. Dikau et al., 1995; Ho et al., 2013) or in combination with other techniques (e.g. Seijmonsbergen et al., 2011). Also, this technique is relatively similar to MPS in that a set of heuristic rules or conditions, representing specific landform classes defined a priori, is used to inform a landform class at unknown locations. Unlike MPS, the rule-base classification does not consider spatial relations between landform units.

The paper is organized as follows. Section 2 describes the geological and geomorphological background of the study area. A description of the MPS technique for mapping landforms, including the configuration of the technique for mapping landforms is presented in Section 3. Mapping results are shown in Section 4; from these, mapping accuracy and the effect of the training area on mapping quality are analyzed and discussed. Conclusions and future perspectives, including general guidelines in applying MPS in mapping landforms are presented in Section 5.

2. Study area

We demonstrate the MPS approach in mapping the landforms in the Buëch Valley, located within the southern subalpine chain of the Dauphiné and Provence Prealps, in the department Hautes Alpes, France (Fig. 1). The Buëch River is a tributary to the Durance River. The mapping site covers an area of approximately 280 km^2, stretching roughly for approximately 20 km along two main tributaries of the Buëch River (Grand Buëch and Petit Buëch), from the town of Aspres-sur-Buëch (Grand Buëch) and Veynes (Petit Buëch) down to some 10 km south of the confluence of these tributaries near the town of Serres. The elevation ranges between 700 and 1800 m (Fig. 1). The geology of the area is characterized by a sequence of sediments from the late Jurassic (Fig. 2; Dumas et al., 1987). The upper-most layer consists of highly-resistant massive limestone of Kimmeridgian–Tithonian age (i.e. Calcaire Tithonique), which overlies alternating layers of limestone and marl (i.e. marno-calcaires) of Argovian age. The bottom layers in the sequence are calcareous black marls deposited during the Callovian and Oxfordian (i.e. Terres Noires; Miramont et al., 2000; Battiau-Queney, 2005). These marl deposits are thick (1500–2000 m)

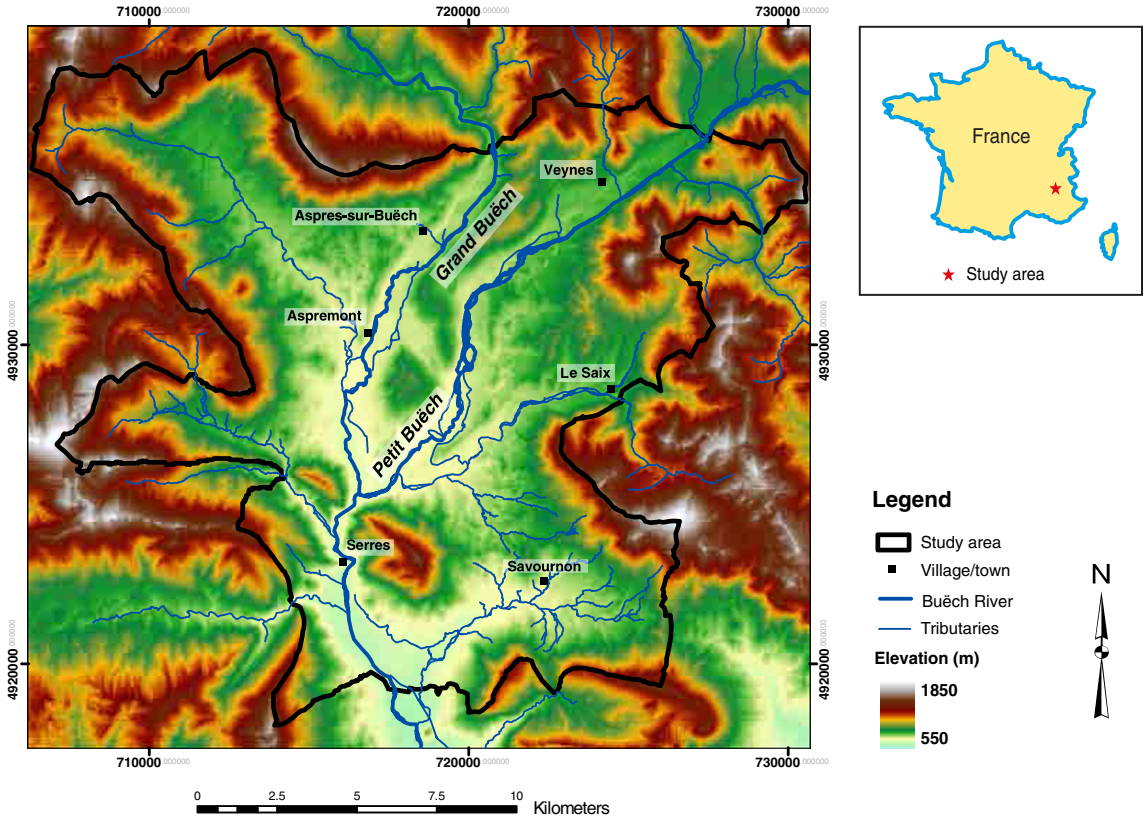

Fig. 1. Location and topography of the study area.

compared to the overlying Argovian deposits (300 m) and Calcaire Tithonique (20–80 m) (Descroix and Olivry, 2002; Brocard et al., 2003). The sedimentary layers were intensively deformed during two subsequent orogenic phases: the Pyreneo-Provencale orogeny from the late Cretaceous to the Eocene with a West–East strike; and the Alpine orogeny in the late Miocene with an NNE–SSW strike. This resulted in a sequence of short folds and thrusts pertaining to these two orogenic phases (Blanchard, 1921; Battiau-Queney, 2005; Brocard and van der Beek, 2006), and a landscape made up of anticlinorial domes and smaller synclinal structures, sometimes at high elevation (synclinaux perchés). The constituent rocks are heavily affected by this deformation by folding and faulting (e.g. diastrophism) and by subsequent weathering during the deglaciation period and the Holocene (Blanchard, 1921). Quaternary deposits are widely found throughout the area, of which the deposits from the last glacial (Würm) period are most prominent. These deposits are largely of glacio-fluvial origin, with material delivered by meltwater streams from the Durance glacier that intruded the Buëch valley at the Freissinouse pass (Brocard et al., 2003). Locally, hillslope deposits from the Holocene can be found.

Present-day geomorphological characteristics (Fig. 2) can be traced back to the late Miocene after the Alpine orogeny. Geomorphological development in the Buëch Valley is strongly linked to differences in lithological resistance to erosion between the massive limestone (e.g. Calcaire Tithonique) and soft marls (e.g. Terres Noires). The Calcaire Tithonique is resistant to erosion, resulting in hogbacks at anticlinal valley sides that tower high above the valley floor. In contrast,

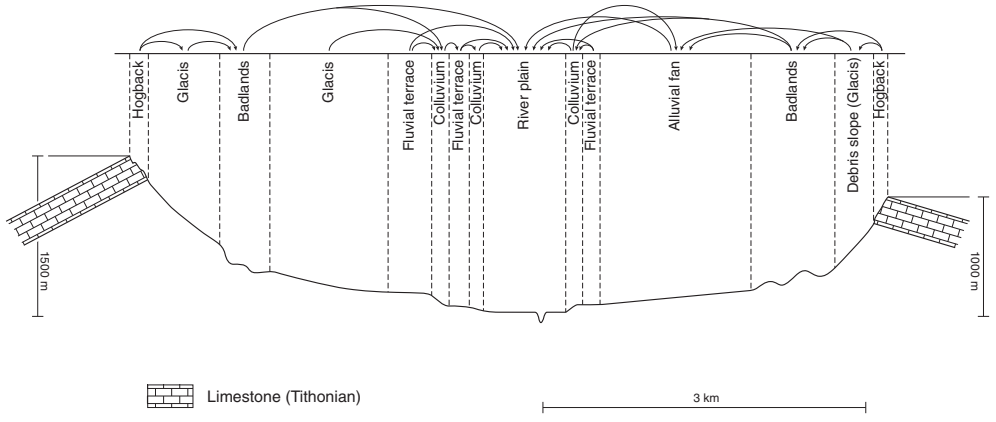

Fig. 2. Schematic presentation of the landform units across a valley in the study area. Arrowheads point toward the landforms that are observed at 10 cells downstream from a landform at the start of arrow lines with a proportion larger than 10% of the total cells of that landform class (Section 4.2.2 and Fig. 9), in the field geomorphological map (Section 4.1). Note that the arrows only provide qualitative information on the relative positions between landforms; and the arrow length does not represent the distances in the landscape. Vertical scale is exaggerated.

the Terres Noires marls show relatively little resistance to erosion. In conjunction with material supplied from the Calcaire Tithonique hogbacks, the Terres Noires marls have given rise to the development of concave, pediment-like slope surfaces (i.e. glacis d'érosion) during the Pleistocene. These glacis d'érosion slopes, referred to as *glacis* hereinafter, have been formed under the influence of frost weathering, solifluction and/or gelifluction when cold, periglacial conditions existed and vegetation was largely absent. Cold conditions then also resulted in large quantities of debris to be transported to the river system, resulting in river valley infilling and raised riverbeds. During a subsequent interglacial period with decreased sediment supply, the river incised, causing the formerly elevated floodplains to become glaciofluvial terraces. With a consecutive alternation of glacial and interglacial periods during the Pleistocene, a sequence of fluvial terraces was successively created at different levels: since large parts of the Buëch Valley were not covered by glaciers, these glacio-fluvial terraces were not eroded by glacier ice and can nowadays be found at elevations of approximately 190 and 80 m above the present-day valley floor (Brocard et al., 2003). Colluviums and alluvial fans in the area stem from the end of the last ice age (Würm), which resulted in progressive accumulation of fine sediments downslope (Descroix and Gautier, 2002). The sharply incised badland topography of certain marl areas was subsequently formed in the Holocene due to high-intensity precipitation, causing severe erosion of the marl deposits downslope. Badlands are prominent landforms in the Buëch valley, responsible for a significant amount of the sediment supply to streams and rivers in the area (Descroix and Olivry, 2002).

3. Methodology

3.1. Field mapping of landforms

A field map of landforms is required to train and validate the automatically created landform map. In this study, we mainly focus on mapping the 'landform complex' (Dramis et al., 2011), which is a sequence of relatively homogeneous entities representing a characteristic morphological pattern of landform elements, for example, debris slopes, alluvial fans, and fluvial terraces. Landform units at this scale can be chosen as model units in a hydrological model (e.g. Vannametee et al., 2013) or as functional units for planning and management (e.g. Arattano et al., 2010).

Following van Asselen and Seijmonsbergen (2006), a map legend was constructed using two criteria: the environment in which landforms were developed (i.e. hillslope or fluvial), and the dominant forming process (i.e. structural control, erosion, or accumulation). This resulted in eight landform classes (Table 1). Hydro-geographical features were also mapped into four classes: *lake* (natural and artificial), *main river*, *perennial stream*, and *ephemeral stream*.

Classification rules or criteria were defined for each landform class. These mapping criteria include locally-observable terrain characteristics and the topographical context observed in the vicinity sufficiently covering the characteristic dimension of the landform units, i.e. approximately 500 m for the landform types mapped in this study (Speight, 1990). The mapping criteria can be grouped into characteristics of lithology (e.g. regolith type, texture, thickness of regolith layer, color, and sorting), topography (e.g. relief, composition and spatial arrangement of landform elements), morphology (e.g. slope angle, aspect, and curvature), vegetation (e.g. type and coverage), channels (e.g. form, pattern, and density), status of geomorphological activity (e.g. active, inactive), dominant geomorphological agents, position relative to the main channel and watershed divide, and relations between different landform types. These criteria were observed and evaluated at approximately 400 locations and the landform class was identified. The topographical map at a scale of 1:10,000 was used as a base map to delineate landform boundaries. This mapping scale is suitable because the typical size of the landform units examined in this study (i.e. $>10^4$ m^2) can be captured at this scale (Speight, 1990; MacMillan et al., 2004; van Asselen and Seijmonsbergen, 2006; Dramis et al., 2011). The field campaign of geomorphological mapping took one month. The mapping procedure started by identifying the hydrological features, particularly the main rivers and perennial streams, because they often indicate the borders between different landform units. The units that can be easily recognized from a long distance, i.e. large-size units or units with a distinct shape (e.g. alluvial fans), were mapped in a subsequent order. Finally, the mapping was done for units with smaller sizes, requiring detailed inspection at a local scale.

3.2. Multiple point geostatistics for mapping landforms

3.2.1. Concept

We use the multiple point geostatistical method developed by Strebelle (2002), which is a single normal equation simulation algorithm often referred to as SNESIM. This MPS approach is a probabilistic technique: the data value (i.e. landform class) at a pixel is simulated based on the discrete probability function of a random variable given a conditioning data event at multiple locations (Honarkhah, 2011). SNESIM is regarded as the first practical MPS algorithm and it has brought the initial MPS concept by Guardiano and Srivastava (1993) into practice (Hu and Chugunova, 2008; Mariethoz and Lefebvre, 2014). In this study, the SNESIM algorithm was implemented in Python, and run in the PCRaster Python framework for stochastic modeling, which has operators on raster maps (Karssenberg et al., 2007). As with other MPS algorithms, SNESIM derives from a training image the statistics of a multiple-point pattern that is used in the mapping phase. In this study, the training data set consists of a field map of landforms and the DEM. In the training phase of the algorithm, the landform class at a location (i.e. pixel) is characterized by a set of topographical properties for that location, taken from the DEM, and landforms at multiple neighboring locations. This information, collected from all pixels in the training area, is used as 'knowledge' to map landforms in other areas where only the DEM is available (Fig. 3). To define the conditional relationships between topographical attributes and landforms, the continuous data (e.g. DEM derivatives) must be converted to categorical variables.

The SNESIM approach generates an automated landform map in two stages: training and mapping (Fig. 3). In the training stage, the SNESIM algorithm visits each cell in the training image and retrieves a set of attributes over the data search template with a central node at the cell visited (Fig. 4), referred to as an attribute pattern. The attribute pattern consists of morphometric attributes, given as categorical values of DEM derivatives (e.g. elevation and slope classes) at the central template node, and landforms at two locations in the downstream direction from the central template node (Fig. 4; Section 3.2.2). The downstream direction is retrieved from a local drainage direction map, in which the flow direction in each cell is assigned to one of its eight surrounding cells with the steepest descending slope in the DEM (Burrough and McDonnell, 2004). The algorithm stores the attribute patterns of all nodes in a search tree structure, i.e. a frequency database, as shown on the right of Fig. 3. This form of data storage results in a fast retrieval of the information in the mapping stage (Strebelle, 2002; de Vries et al., 2009).

In the mapping stage, the order in which the cells in the mapping area are sequentially visited is specified first (Section 3.2.5). The algorithm visits the cells in this order, executing the following three steps for each cell. First, the algorithm retrieves the attribute pattern in the template centered at the cell visited, which includes the DEM attributes of the central template node and the landforms at its downstream locations (in case neighboring cells have already been visited and mapped). Second, the frequencies of each of the landform class occurrences (i.e. number of cells) conditioned to the attribute pattern observed in the template are retrieved from the search tree. This

Table 1
Descriptions of the landform classes used in landform mapping.

Geomorphological environment	Process	Landform class	Descriptions		
			Topography/morphology	Material deposits	Vegetation/landuse
Hillslope	Structural control	Hogback	Steep ridge or cliff (60–80°) of bare rock as a result of lithological resistance to erosion. Located at the highest position in the landscape as a stretching rocky belt with narrow width along the mountain crest or watershed divide in a perpendicular direction to the slope.	Highly-resistant massive limestone. Absence of material deposits or soil layer due to steepness.	No vegetation, or short grasses or shrub vegetation.
	Erosion	Badlands	Intensely dissected terrain with extensive branches of interconnected sharp ridges, forming local watershed divides and V-shaped gullies with steep side slopes (>65°). Slopes are highly incised by small rills showing high drainage density as a result of intensive erosion by overland flow. Mostly bordered by deep-cut ephemeral channels. Situated at a variable height in the landscape.	Very thin layer of dark-color marls or clay with high weathering degree. Relatively impermeable and erodible.	Absence or sparse vegetation (<10%), of which short grass, shrubs and coniferous tree are the most common species. Agricultural activities not present.
		Glacis	Concave slope surface, narrow and elongated, with decreasing slope angle from 25° to 3° in downstream direction. Situated at a relatively high position in the landscape, but not always connected to the mountain crest. The lower part might be disconnected from the main part due to erosion, resulting in low-relief isolated hills with flat top. Badlands often present at the side or at a lower part.	Relatively thin deposit layer with increasing thickness downslope (i.e. 0.5–2 m). Moderately-sorted angular clasts with relatively fine matrix; boulder-size materials	Mainly forest. Deciduous species at low elevation and coniferous species at high elevation.
	Accumulation	Debris slope	Extensive rectilinear slope surface with slope angle between 25°–40°. Positioned high in the landscape, below mountain crests or hogbacks. Mass movements are included in this class.	Heterogeneous matrix-rich deposit, consisting of loose and angular materials of limestone fragments, mostly eroded from higher elevation and crudely stratified. Thickness of deposit up to 10 m.	Lack of vegetation at the steep part while densely-vegetated in moderate to low lying slope (<25°).
Fluvial	Accumulation	Alluvial fan	Fan-shape landform with a convex cross-sectional profile across the main slope, usually covering a large area of up to a few km^2 with gentle slope gradient varying from 0.5° to 20°. Developed at a relatively low position in the landscape at the foot of a steep slope with an abrupt transition of slope gradient. Deep-incised streams at lateral boundaries.	Well-developed soil layer, heterogeneous and poorly-sorted materials dominated by fine-grained marls or calcareous debris particles. Decreased grain size along the slope. Thickness of deposits between 1 and 10 m	Grassland and intensive agricultural activities.
		Colluvium	Deposits without a clear fan shape and source areas. Situated directly at the foot of moderate to steep slopes. Often laterally interconnected. Slope profile slightly concave.	Materials are generally composed of abundant angular gravel within a finer matrix. Internal structures poorly developed to absent.	Grassland, light density forest. Agricultural activities can be found.
		Fluvial terrace	Elevated plane of flat surface slope with sharp-cut boundary (i.e. steep side slope). Developed along the main valley parallel to the main river. Position variable in the landscape, higher than the present-day river level. No longer flooded by the river.	Relatively fine grains (i.e. sand and silt) with rounded gravel. Moderately to well sorted. Variable deposit thickness, usually >0.5 m.	Grassland, shrubs, and forest. Agricultural activities can be found
		River plain	Low-lying flat terrain unit bordering the main river channel or permanent streams at the same or slightly-higher elevation. Regularly or yearly flooded. Relatively unclear boundary with the landforms at a higher position (e.g. colluviums).	Similar to fluvial terraces. Sedimentation process still active. Gravel bar present.	Forest, shrub, grassland, or no vegetation. Small agriculture activities.

information is converted into a categorical probability distribution giving the probability of landform classes at the cell visited:

$$\text{Prob}\{I(i,g)|\mathbf{V}_i\} = \frac{f_{(\mathbf{V}_i|g)}}{f_{(\mathbf{V}_i)}} \quad (1)$$

where $I(i,g)$ is the event that the cell i belongs to the landform class g, $\mathbf{V}_i$ is the vector containing the attribute pattern observed at location i: $f_{(\mathbf{V}_i)}$ is the number of cells in the training area with the attribute pattern $\mathbf{V}_i$, and $f_{(\mathbf{V}_i|g)}$ is the number of cells in the training area with the attribute pattern $\mathbf{V}_i$ that belong to the landform class g. In the third and final steps, a realization of the landform class is drawn from this probability distribution and assigned to the cell visited. The algorithm then moves to the next cell in the predefined sequential order and repeats the mapping procedure. This is done until all cells in the mapping area have been assigned a realization of a landform class.

In case the attribute pattern $\mathbf{V}_i$ observed at the target mapping cell does not exist in the database (e.g. attributes are missing or not observed in the training images), the last attribute in $\mathbf{V}_i$ will be disregarded, resulting in a new attribute pattern. This attribute trimming process is done until the trimmed attribute pattern matches an attribute pattern in the frequency database. Then, the numbers of cell occurrences with respect to this trimmed attribute pattern are retrieved and converted into the categorical probability distribution of landform classes to be used in mapping. If the entire set of observed attributes $\mathbf{V}_i$ does not match the attribute patterns observed in the training area

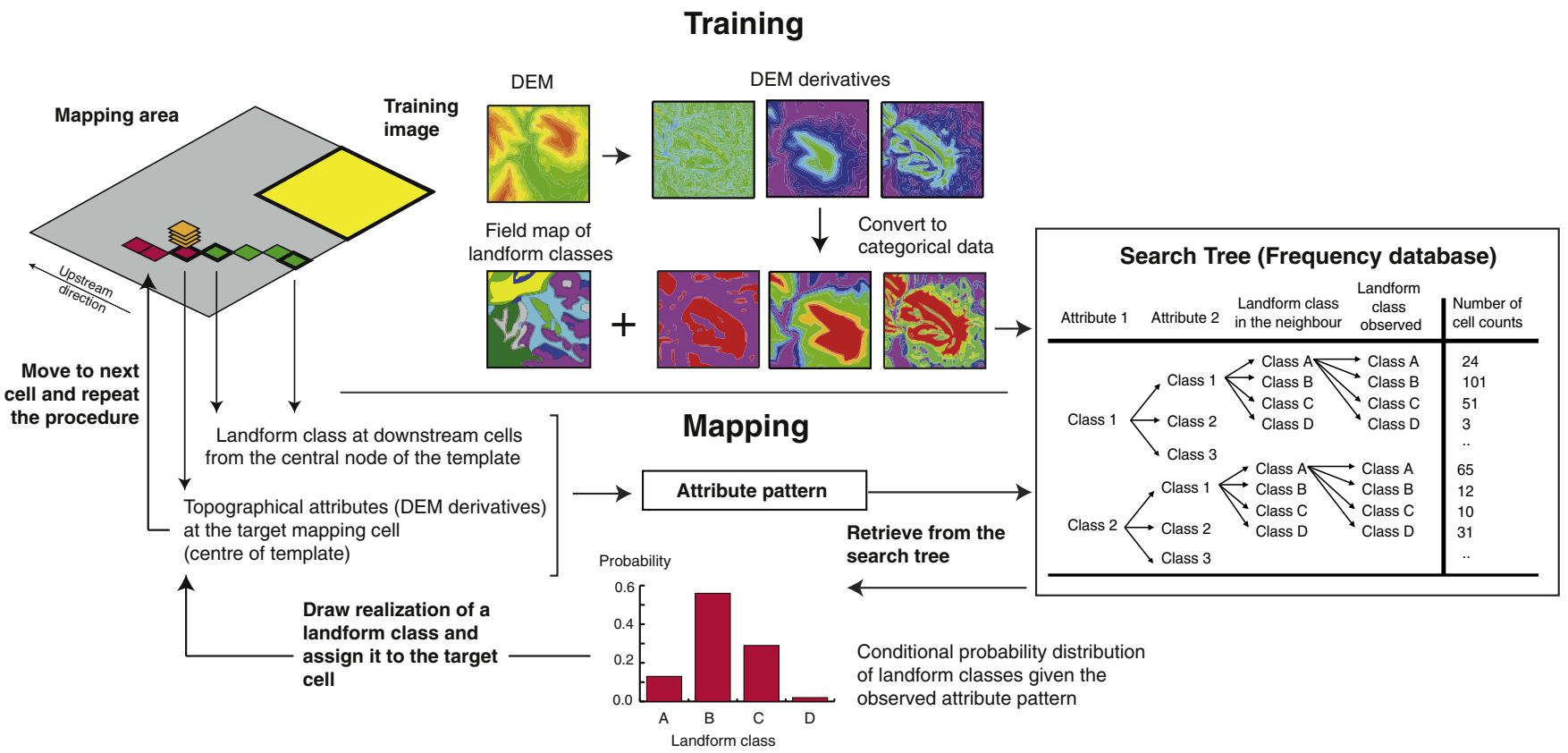

Fig. 3. Schematic representation of the MPS concept for mapping of landforms. The mapping procedure consists of two steps; training (above) and mapping (below). The search tree as a frequency database (right) is created for the training stage, providing probability distributions of landform classes conditioned to certain attribute patterns, which are used to map the landforms outside the training area. Note that, due to a limited space, we only present, in the search tree, the relations of four landform classes (i.e. A to D) given three attributes; two morphometric attributes discretized into two and three classes, and one non-morphometric attribute (i.e. a landform in the neighborhood). Data search template is shown in Fig. 4.

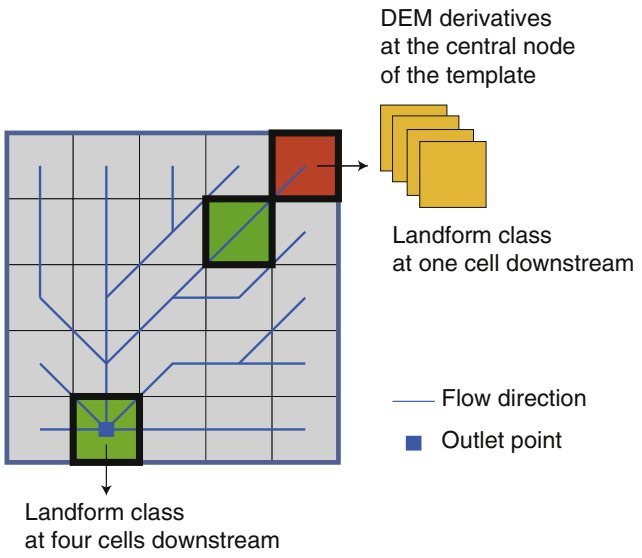

Fig. 4. Mapping areas of 5 × 5 cells and data search template used in this study (bold cells). The template consists of the central node (red) and cells at two locations downstream of the central node (green) (i.e. immediate downstream neighbor, and 10 cells downstream from the central node). Cell drainage direction is shown in blue lines. The attribute pattern for each node consists of a set of local DEM derivatives and landforms at one and 10 cells downstream. Note that, due to a space limit, a template with four cells instead of 10 cells downstream from the central node is shown.

(i.e. all attributes have been dropped out), a probability distribution of landform classes over the entire training area (i.e. marginal probability distribution) will be calculated and used in mapping.

To ensure reliable statistics, the attribute patterns used in mapping should have enough replicates (i.e. cell counts) in the training image (Liu, 2006). In this study, a minimum number of replicates allowing an attribute pattern to be used in mapping are set to five. This value was derived based upon a number of test runs. If this condition is not satisfied, attributes in the observed attribute pattern are dropped one-by-one, until the number of cells corresponding to the new attribute pattern is equal to or above five.

Since the MPS technique assigns to the cells a realization of a landform class drawn from a conditional probability function, the landform class assigned to the given cells may vary from one map realization to another. Thus, the landform mapping has to be done in a stochastic Monte Carlo framework, in which a number of different equally likely map realizations are generated and used to derive the final landform map, which contains for each cell the most often occurring landform class in the cell, calculated over all map realizations. In addition, this stochastic framework allows calculating uncertainty in the map (Section 3.3.1). The Monte Carlo procedure has been run by generating 35 map realizations. Test runs with a larger number of realizations gave comparable results, indicating that the 35 realizations are sufficient.

3.2.2. Attributes used in mapping

We investigate the suitability of four morphometric and two non-morphometric attributes for mapping landforms in the study area (Table 2). These attributes are chosen analogous to the criteria used in field mapping (Section 3.1). Morphometric attributes are derived from a 37.5 m resolution DEM. These attributes are retrieved from the same location as in the field map of landforms, i.e. at the central node of the data search template (Section 3.2.1, Fig. 4). Three of the morphometric attributes used, elevation, slope gradient, and profile curvature, are among the most fundamental attributes that are considered as sufficient in characterizing and discriminating different landform types (Hammond, 1964). These attributes are, thus, commonly chosen for automated landform classification (e.g. MacMillan et al., 2000; van Asselen and Seijmonsbergen, 2006; Gharari et al., 2011). Note that elevation used in this study is the relative elevation to the regional base level, i.e. elevation at the nearest river to which cells drain, or the lowest elevation in sub-catchments (Rennó et al., 2008). In addition, slope variability is used to represent topographical roughness around the cell of interest.

Non-morphometric attributes in the neighborhood (i.e. landform classes) are used to represent the spatial patterns of landform units in the landscape. We consider landforms at two locations, i.e. at the direct downstream neighbor of the central template node, and at 10 cells downstream (i.e. 375–530 m) from the central template node following the drainage path. A group of cells in proximity is likely to belong to the same class of landform; as such a landform at the adjacent location is a good indicator to determine a landform at a location of interest. This information can also help in maintaining the spatial continuity of mapped landform features. Landforms have a structure of organization across the landscape; certain landforms coexist resulting in a sequential formation of landform units along the hillslope (Fig. 2). A landform at 10 cells downstream from the central template node is used to represent a landform at the lower boundary of the landform at the cell of interest, giving positional relations between landforms (Section 4.2.2).

3.2.3. Class numbers and class boundaries of morphometric attributes

SNESIM requires the use of categorical variables to create the frequency database (Section 3.2.1). The number of classes and class boundaries for discretization of continuous morphometric attributes was selected based on the zonal statistics of DEM derivatives for each landform class calculated over the entire study region. Class boundaries were manually defined such that each of the resulting attribute classes represents a single or a small number of different types of landforms. We kept the number of classes at a minimum, because increasing

Table 2
Attributes used in geomorphological mapping.

Type	Attributes	Symbol	Descriptions/remarks
Morphometric	Height above the nearest drainage	*HAND*	Adjusted terrain height relative to the elevation at the nearest channel to which a cell drains (Rennó et al., 2008; Nobre et al., 2011). The channels, as a reference elevation level, are defined as cells with the upstream area exceeding 2 km^2 (i.e. 1500 cells). A cell drainage direction is calculated based on the elevation data using the eight-point pour algorithm (Burrough and McDonnell, 2004).
	Slope gradient	S	Absolute change in height per distance in horizontal direction; a value between 0 and 1, calculated over a window of 3 × 3 cells using the third-order finite difference method (Skidmore, 1989).
	Profile curvature	φ	Change in slope gradient per distance in horizontal direction along direction of the slope (Zevenbergen and Thorne, 1987). Negative at concave slopes and positive at convex slopes.
	Slope variability	S_{var}	Absolute difference between the minimum and maximum slope gradients over certain areas (Ruszkiczay-Rüdiger et al., 2009), obtained over a 7 × 7 cell window (i.e. about 0.07 km^2).
Non-morphometric	Landform at one cell downstream	G_1	A landform at a close proximity to the cell of interest, located at an adjacent downstream position.
	Landform at 10 cells downstream	G_{10}	A landform at a cell located 10 cells (375–530 m) away from a cell of interest in the downstream direction along the local drainage direction map.

the number of classes leads to a larger number of different attribute patterns in the frequency tree, resulting in a smaller number of replicates per attribute pattern. A small number of replicates should be avoided, as this reduces the reliability of the conditional probability functions represented by the frequency tree.

3.2.4. Training images

Training images should contain sufficient information on the characteristics and spatial pattern of landforms present in the mapping areas. In this study, we select a training image covering an area of 28 km^2 or 10% of the study area. The training image consists of four circular areas, each of which has a diameter of 3 km (i.e. 80 cells) and size of approximately 7 km^2. This size is chosen based on an assumption that field mapping of landforms could possibly be done by one or two persons in a short time period. Also, the dimension of a single training image sufficiently covers the characteristic length of most landform units, including the spatial pattern of landforms (Fig. 5). Although large and elongated landforms (i.e. debris slopes and river plains) may not be entirely captured within the training image, the position of these units relative to other landforms is well represented. These four areas are randomly located over the study region to account for the spatial variability in landform characteristics and to increase the statistical reliability in the training data sets (Fig. 5). Landform mapping using this training image is referred to as the 'base' mapping scenario.

We also examine the effect of the size of training images on mapping quality since the amount of information used in mapping is strongly related to the size and coverage of the training images. A set of mapping scenarios with different sizes of training images is created. This is done by dropping out at least one of the four training areas used in the base mapping scenario. This results in 16 mapping scenarios with training image sizes ranging from 7 to 20 km^2 or 2.5–7.5% of the total area. Accuracy of the auto-generated landform maps is expected to be related to the size of the training images used in mapping.

3.2.5. Path of cell visit in mapping

SNESIM visits the cells in a sequential order in the mapping stage. Landforms that have been previously mapped in the nearby pixels will be conditions to map the cell under a current visit. In this way, the path of cell visits may have a strong influence on the mapping quality as it is directly related to the information content used in mapping (Liu and Journel, 2004). Here, we investigate two different cell mapping orders, i.e. one on a random basis and one along the local drainage network in upstream direction. For the latter approach, landforms at the downstream cells will be initially mapped, providing hard conditions for mapping the landforms at the upstream cells. The path of cell visits that results in a higher mapping quality is chosen and used throughout the study.

3.3. Evaluation of the MPS technique

3.3.1. Uncertainty in the mapping results

Variation of landform classes mapped at a cell over map realizations can be quantified using the index of qualitative variation (Gibbs and Poston, 1975):

$$q_i = \frac{G_i}{G_i - 1}\left(1 - \sum_{g=1}^{G_i} p_{g,i}^2\right) \quad (2)$$

where q_i is the index of landform variation mapped at cell i, $p_{g,i}$ is the proportion of realizations with a landform g that is assigned to cell i, and G_i is the total number of landform classes assigned to cell i. The index varies between 0 and 1, indicating, respectively, that a single

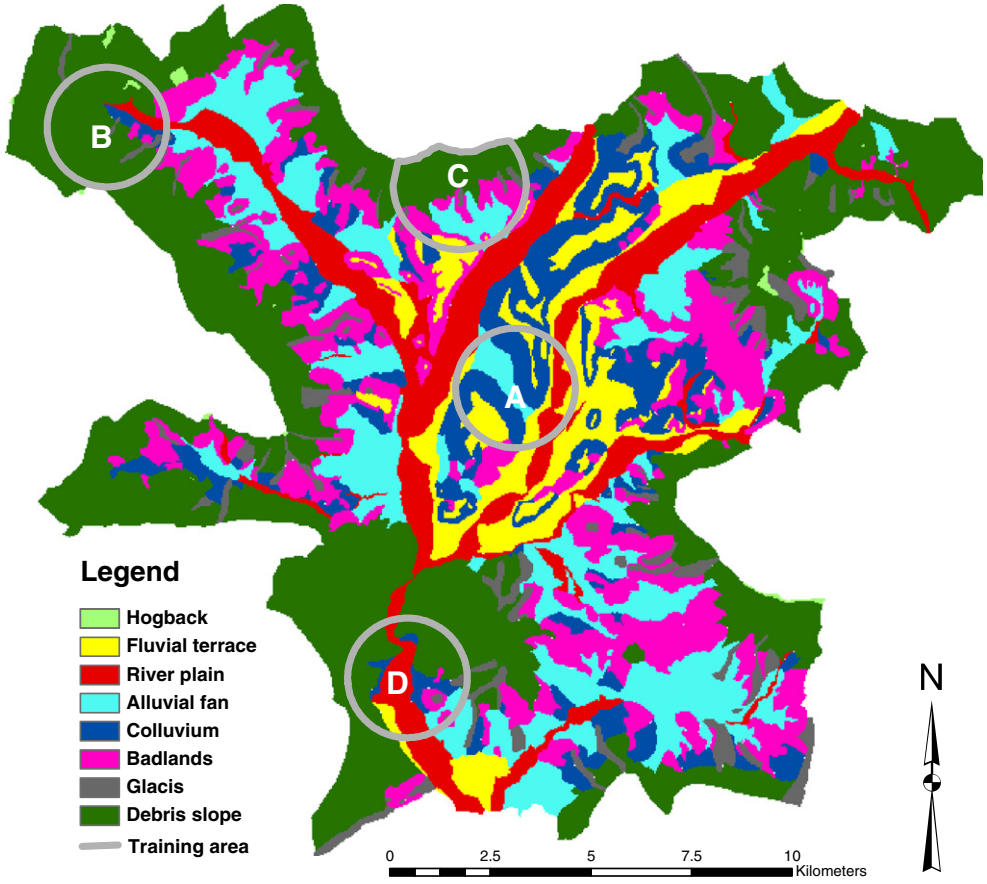

Fig. 5. Field map of landforms; rasterized to a 37.5 m cell size. Hydrological features are not shown. The training areas (A to D) are indicated with circles.

landform class is observed over all map realizations, and a low mapping uncertainty; and that all landform classes are evenly assigned across all map realizations and a high uncertainty in mapping.

3.3.2. Mapping accuracy

The accuracy of the landform maps produced from the MPS technique is evaluated against the field map of landforms obtained in Section 3.1. It is assumed that errors of field-mapped landforms are relatively small and do not have a significant effect on the evaluation results. Evaluation of the mapping accuracy is done for the final landform map for each mapping scenario, separately for the area outside the training area used in the base scenario (i.e. all training images), and for the training area itself of the respective scenario. The latter is done to retrieve information on the possible maximum mapping accuracy when there is no discrepancy between landform characteristics in the training and mapping areas. The quality of the automated map is evaluated per pixel and over a group of adjacent pixels.

For a pixel-based evaluation, the fraction of correctly classified cells and the kappa statistics are used. The kappa coefficient (κ) is computed as (Lillesand et al., 2004):

$$\kappa = \frac{p_a - p_e}{1 - p_e} \tag{3}$$

where p_a is the fraction of correctly classified cells, and p_e is the overall probability of random agreement among landform classes whose cells are mapped both correctly and incorrectly. The kappa coefficient ranges from 0 to 1. A value of 1 represents a perfect agreement between two maps, and 0 corresponds to an agreement that would only be obtained by chance.

Evaluation of mapping quality over a group of contiguous pixels is done using two criteria. First, we evaluate the degree of landform similarity between the automated and field maps, for every cell location, over a template of 4 × 4 pixels (150 × 150 m). This is calculated as (Pontius et al., 2004):

$$s_i = \sum_{g=1}^{G} min\left(f_{g,i}^{A}, f_{g,i}^{F}\right) \tag{4}$$

where s_i is an index of landform similarities over a window with a central location i, g is a landform class (= 1,…,G, with G the total number of landform classes observed in the study area), $f_{g,i}$ is a fraction of cells with a landform class g over the window with a central location i, the superscripts A and F indicate the automated map and field landform map, respectively, and $min(x,y)$ selects the lesser value of x and y. The index of cell similarities ranges between 0 and 1. A value of 0 means that landform classes over the window between the two maps are totally different, while a value of 1 indicates identical landforms between the two maps. Total landform similarity can be obtained by averaging the index of similarity over the whole map.

Second, we evaluate the average difference D_i (m^2) in the size of landform units between the automated and the field maps (Hagen-Zanker, 2006). This metric is calculated as follows. First, areas (m^2) of contiguous patches (i.e. representing single landform units) are retrieved and assigned to the cells that belong to the units. The cell values are, then, distance-weighted averaged using a search radius of 4 cells. These are done for both the automated and field maps. In the next step, these two maps are subtracted to result in a new map representing cell-by-cell differences in the weight-averaged unit sizes. These values are, then, averaged over the whole map to retrieve the average difference in unit sizes between the automated and field maps. This calculation was made using the Map Comparison Kit software package (Visser and de Nijs, 2006). A positive value of D_i indicates that the average size of landform units in the automated map is larger than that of the field map, and a negative value means the opposite.

3.3.3. Performance relative to the rule-based classification approach

To evaluate our mapping algorithm, the automated maps generated by MPS are compared to those from a rule-based classification, which is a widely used automated technique (e.g. Ho et al., 2012, 2013). Here, the classification procedure is set up in a similar manner as MPS. The classification rules are defined as combinations of different attributes discretized into classes; each combination describes the characteristics of a particular landform. We only use morphometric attributes (Section 3.2.2) to define the classification rules, neglecting the non-morphometric attributes in the neighborhood. Thus, the classification is only based on statistics of attributes at the target mapping cells without considering spatial relations between cells. The classification rules are heuristically derived from the statistical analysis of attributes for each landform class sampled in the training image. Distribution characteristics of morphometric attributes for different landform classes are analyzed to identify the attribute values that enable discrimination between landform classes. This is done in a hierarchical order for each mapping attribute. *HAND* is used as the first condition, followed by slope gradient, profile curvature, and slope variability. This results in a classification tree whose lowest branches (i.e. rules) represent single types of landform. With these heuristic rules, the landform class in each pixel is identified deterministically. Note that class numbers and class boundaries chosen for morphometric attributes in the rule-based classification are different from those used in the MPS.

4. Results

4.1. Field map

The Buëch valley (Fig. 5) is dominated by debris slopes and badlands (16%) (Table 3). *Hogback* is the least present landform type (0.2%).

Landforms show a sequential organization from the mountain crest to the valley bottom, as shown in the schematic cross section of Fig. 2. Hogbacks occupy the highest position in the landscape, below which debris slopes extend over the upslope part. Glacises are generally

Table 3
Percentage of landform units in the training images and mapping areas.

Area	Area coverage (km^2)	Percent to the total area	Label of training image*	Landform classes							
				Hogback	Fluvial terrace	River plain	Alluvial fan	Colluvium	Badlands	Glacis	Debris slope
Training	7	2.5	A	0	29.0	14.6	14.8	40.8	1.0	0	0
	7	2.5	B	0.7	0	5	0	5.6	3.6	4.0	81.0
	7	2.5	C	0	4	0	19.7	0.7	23.5	4.0	48.0
	7	2.5	D	0	3.7	25.2	5.6	10.8	5.4	2.4	46.9
	28	10	A + B + C + D**	0.2	9.1	11.2	10.0	14.6	8.3	2.6	44.0
Mapping	247.6	90	–	0.2	7.5	11.3	14.2	9.4	17.2	4.7	35.5
Total	275.6	100	–	0.2	7.6	11.3	13.8	9.9	16.3	4.5	36.3

*Referred to the label of area in Fig. 4.
** Combination of all training images: A to D (i.e. base scenario).

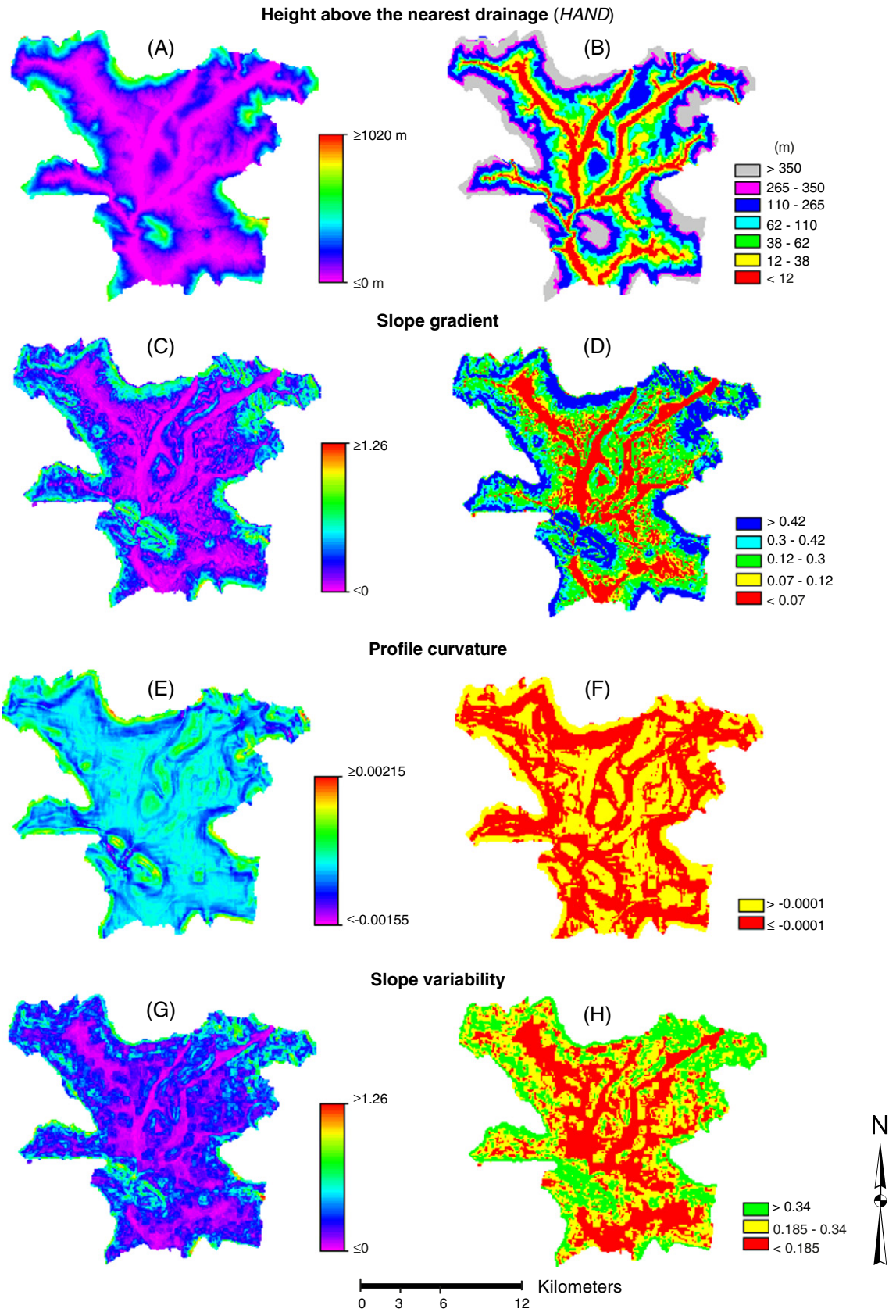

Fig. 6. Morphometric attributes shown in numeric (A, C, E, G) and discretized into classes (B, D, F, H). The number of classes and class boundaries for each attribute are chosen to allow the best discrimination between landform classes (see Fig. 8).

found at approximately the same elevation as debris slopes, and are sometimes still connected to hogbacks at their upper boundaries. Badlands and colluviums are typically positioned below the debris slopes and glacises. River plains are present at the valley bottom, surrounded by elevated plains of fluvial terraces and alluvial fans. This sequence of landform classes suggests that the relative elevation and position of units over a slope profile between the watershed divide and streams are of importance in characterizing the landforms.

The proportion of landform units in the training area of the base scenario (i.e. A to D combined, Table 3) is slightly different from that of the area outside the training image (i.e. mapping area). The proportion of landform classes in individual training areas (i.e. A, B, C, and D separately, Table 3) shows quite some variation.

4.2. Analysis of mapping attributes

4.2.1. Morphometric attributes

The morphometric attributes (Fig. 6A, C, E, G) are positively and moderately correlated (Table 4), indicating that the attributes partly contain similar information. However, each attribute carries specific information that, when combined, is expected to be valuable in the automated mapping process.

The landforms in the fluvial environment (*river plain*, *fluvial terrace*, *alluvial fan*, and *colluvium*) have comparable mean morphometric attribute values (Fig. 7A). The range of variation of morphometric attributes is however small, resulting in limited overlap between these landform classes, implying that the landforms can possibly be distinguished, despite their similarity in mean values (Fig. 8). A landform class can often be distinguished from the others using a single morphometric attribute. For example, *HAND* is the most useful attribute to distinguish *river plain* from other landform classes because the river plains are situated at the lowest position in the landscape and have the lowest *HAND* value. However, *alluvial fan* and *fluvial terrace* are an exception, as morphometric characteristics of these two landform classes considerably overlap (Fig. 8). Discrimination between *alluvial fan* and *fluvial terrace*, using these morphometric attributes alone, is expected to be difficult.

Morphometric properties of landforms in the hillslope environment (*debris slope*, *glacis*, *hogback*, and *badlands*) are clearly different from those in the fluvial environment. *HAND* appears to be the most important attribute capable of distinguishing units as the mean values differ between landform classes in the hillslope environment (Fig. 7B). However, Fig. 8 shows that morphometric properties of landforms in the hillslope environment exhibit large variation and overlap between landforms, i.e. morphometric properties of *debris slope* significantly overlap with *glacis* and *hogback*. However, *debris slope* can possibly be discriminated from *badlands* using *HAND* and slope gradient.

4.2.2. Non-morphometric attributes

Non-morphometric attributes, i.e. landforms at downstream locations from the cell of interest, provide additional information to distinguish between landform classes. A landform at the immediate downstream neighboring cell is mostly identical to the landform at the target cell (results not shown). However, this is exceptional for *hogback* where the direct downstream cells are of other landform types, mainly *debris slope*. This is due to the small size and elongated shape of *hogback*, extending along watershed boundaries (Table 1).

Landforms at a location of 10 cells downstream along the local drainage network from the cell of interest (Fig. 9) often correspond to the immediately next landform class in the top-down landform sequence shown in Fig. 2. However, for very large landform units (i.e. *alluvial fan* and *debris slope*), a distance of 10 cells downstream may not be sufficient to retrieve the landform at the adjacent downstream neighbor.

Landform classes located 10 cells downstream from the cells of interest can be explained by the processes during landscape evolution (Section 2). There is a dominating landform class at 10 cells downstream for some landform types. For example, the majority of landform classes observed at 10 cells downstream from the *fluvial terrace* cells is *river plain* (i.e. 50% of the *fluvial terrace* cells; Fig. 9A). This is because *fluvial terrace* and *river plain* are both found in the river valleys, often neighboring each other, where *river plain* is by definition at a lower elevation and thus often occurring 10 cells downstream from *fluvial terrace*. So, a landform at a 10 cell downstream location is an important criterion to distinguish *fluvial terrace* from other landform classes in the fluvial environment. Generally speaking, non-morphometric attributes in the surroundings (i.e. landform types) provide additional information where morphometric attributes alone are insufficient in distinguishing between landforms.

Table 4
Correlation coefficients between morphometric attributes used in mapping.

Attributes	Correlation coefficient			
	HAND	*S*	φ	S_{var}
HAND	1	0.68	0.53	0.5
S	–	1	0.25	0.6
Φ	–	–	1	0.23
S_{var}	–	–	–	1

Referred to the symbols used in Table 2.

4.3. Configuration of the MPS technique

4.3.1. Defining class boundaries for morphometric attributes

The MPS technique requires the attribute values to be discretized into classes (see Section 3.2.3, Fig. 6B, D, F, H). The analysis of the four morphometric attributes used in this study has shown that *HAND* and slope gradient are key attributes in distinguishing different landform classes. In this study, *HAND* and slope gradient are classified into seven and five classes, respectively (Fig. 8A, B). Landforms in the fluvial environment correspond to narrow ranges of variation in *HAND* and slope gradient (see Section 4.2.1). Narrow class intervals were, therefore, chosen for low attribute values. On the other hand, given the large ranges of variation in *HAND* and slope gradient observed in the hillslope environment, coarser class intervals were used for higher attribute values. The two other morphometric attributes, profile curvature and slope variability, do not show a large capability of discriminating between landform classes. Here, we used low class numbers for these attributes; two classes for profile curvature and three classes for slope variability (Fig. 8C, D).

4.3.2. Order of cells in mapping

The order used in visiting cells during automated mapping (Section 3.2.5) affects the mapping results. Mapping the cells on a random basis results in map realizations with excessive noise (Fig. 10A). On the other hand, the mapped landform units are more spatially contiguous when cells are visited and mapped in an upstream direction along the drainage network (Fig. 10B). Results from the base mapping scenario (i.e. Section 3.2.4) show that the average difference in unit size, D_i, between mapping realizations with different orders of cell visit is between 1 and 4 km^2. The average number of attributes used in mapping of a cell is 4.7 when the cells in the map are randomly visited. This number increases to 5.6 when cells are mapped along the drainage network. This finding indicates that, with a random cell mapping order, non-morphometric attributes are not fully used during the mapping process because landforms at downstream locations may not be available (i.e. cells are not visited and mapped). Thus, information used in mapping is mostly limited to the morphometric attributes. This has the main disadvantage that the spatial relation between landform units in the landscape is not used in mapping, resulting in noise in the automated maps, which reduces mapping accuracy, and particularly causes errors in average unit size between the automated and field maps. Based on a single map realization, the fraction of correctly-mapped cells using four attributes (only morphometric attributes used) is 0.35, while this fraction increases to 0.55 for cells that are

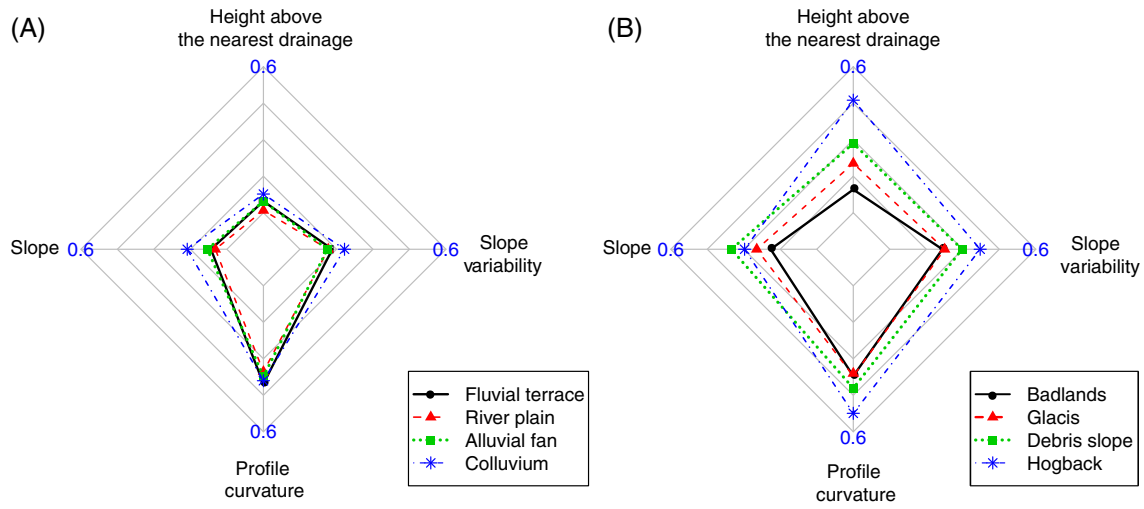

Fig. 7. Comparison between the mean values of normalized morphometric attributes to a range of 0–1, for different landform units. A) Fluvial environment, B) hillslope environment. The axis of the spider plots is set between 0 and 0.6.

mapped using six attributes (i.e. landforms in the neighborhood are used). These results show that the non-morphometric attributes in the neighborhood are beneficial and should be used in mapping. However, using the path of cell visits along the drainage network may result in artifacts of simulated landform features, i.e. straight lines along the flow direction (Fig. 10B). These artifacts are caused by propagation of mapping the same landform class in the upstream direction when a landform at a direct downstream neighbor is used in mapping (i.e. a landform at the direct downstream neighbor is often the same type as a landform at the target cell; see Section 4.2.2). These artifacts can be minimized by aggregating a large number of map realizations. We selected the option of cell mapping along the drainage path for all scenarios, as it results in a higher mapping quality than randomly visiting cells.

4.4. Mapping results

4.4.1. Overall mapping quality

Individual map realizations show considerable variation in the landform class mapped at a particular cell (Fig. 10); in the base scenario 30–35% of cells in the area do not have the same landform class for all realizations. The index of cell similarity over 4×4 windows between map realizations, s_i (Eq. (4)), is 0.76, i.e. the value averaged over the map. The variation in landform classes mapped at cells, evaluated over all map realizations, is quite large in low-lying areas and mid-level positions in the landscape (Fig. 11), indicating a large uncertainty in mapping landforms in these areas. Mapping uncertainty is somewhat smaller at higher elevations. A single class of landform is mapped at many locations in this area (i.e. $q_i = 0$; Fig. 11). The probability of the most occurring landform class at cells (Fig. 12) is typically small for cells close to the unit boundaries, while this probability gradually becomes larger toward the center of units. This probability pattern indicates an uncertainty in defining the boundaries between landform units, as the cells at this location may exhibit characteristics that can be considered as belonging to multiple types of units. Thus, the cells cannot always be classified as a certain landform class in every map realization.

In the base scenario, the percentage of correct cells and the kappa coefficient for individual map realizations are 48.6 ± 0.6% and 0.34 ± 0.05, respectively. The index of cell similarity (Eq. (4)) ranges between 0.51 and 0.53. The average unit size of individual map realizations is somewhat larger than the field map with D_i values of 1.35–3.60 km^2. The overall accuracy of the final map (Fig. 13) is slightly better than that of a single map realization. The percentage of correct cells increases to 51.2%, with a kappa coefficient of 0.37. The index of cell similarity also increases to 0.54. However, the quality of the final map with regard to the unit size is slightly lower than that of individual map realizations, with D_i increasing to 4.6 km^2.

There is considerable spatial variation in the mapping accuracy. Cells located at a high elevation near local watershed boundaries are mapped with a higher accuracy than cells at lower elevation. The automated map also exhibits a larger degree of similarity with the field map at higher elevations (Fig. 14A). The probability in mapping the correct landforms at cells even reaches unity at many high-elevation locations (Fig. 14B), mainly because usually only one type of landform (*debris slope*) is found at high elevations. Mapping accuracy is relatively low in areas at mid-slope positions and near the main river. In these areas, different landforms that have overlapping morphometric and non-morphometric properties can be observed (see Section 4.2). Accordingly, the degree of cell similarity in these areas is also quite small (Fig. 14A).

4.4.2. Mapping quality per landform class

The landform classes are different regarding the mapping accuracy. Because the results for the different criteria are comparable, we focus on the mapping quality as presented by the percentage of correct cells for the base mapping scenario. The class *debris slope* can be mapped with the highest accuracy. It is shown that 90% of the debris slopes in the field map are correctly mapped (i.e. Producer's Accuracy), while 75% of the *debris slope* cells in the automated map truly represent debris slopes in the field (i.e. User's Accuracy) (Table 5). The accuracy of mapping *debris slope* corresponds well with the spatial pattern in mapping uncertainty. Figs. 11 and 14B show that *debris slope* is mapped with a high certainty (i.e. $q_i = 0$) and that a large number of these *debris slope* cells in the automated maps are correct (probability of a correctly-mapped landform class of 1). As noted, *debris slope* is the dominating landform class in the higher part of the landscape. Thus, mapping the debris slopes in this area is relatively straightforward. *Alluvial fan* is the second most accurately mapped landform class in this study (Producer's Accuracy of 57%). However, the proportion of alluvial fans in the automated map that really represent alluvial fans in the field is smaller (User's Accuracy of 34%). This indicates an overestimation of *alluvial fan* in the automated map. A large mapping accuracy of *alluvial fan* may be partly due to this overestimation. Other landforms are mapped with Producer's Accuracies below 35%.

Mapping accuracy is lowest for *hogback*. It is shown that *hogback* is scarcely present in map realizations, and totally absent in the final map (Fig. 13). This is due to the small proportion of hogbacks present in the training image. With a small number of cell counts in the frequency database, probability of *hogback* under any attribute conditions is low. As a result, the cells tend to be misclassified to other landform

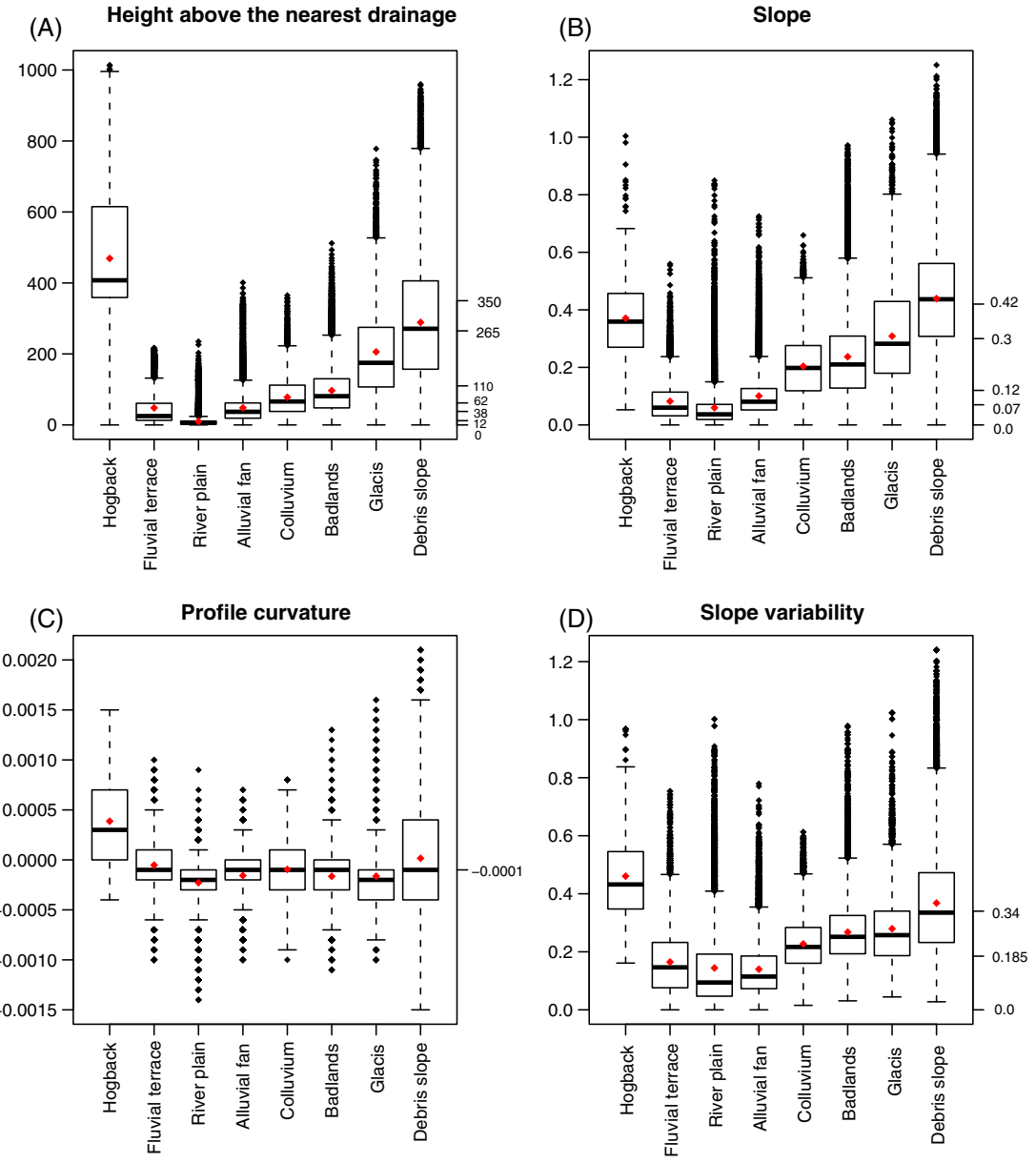

Fig. 8. Box plots showing statistical properties of morphometric attributes for different landform classes, with the class boundaries indicated on the second axis.

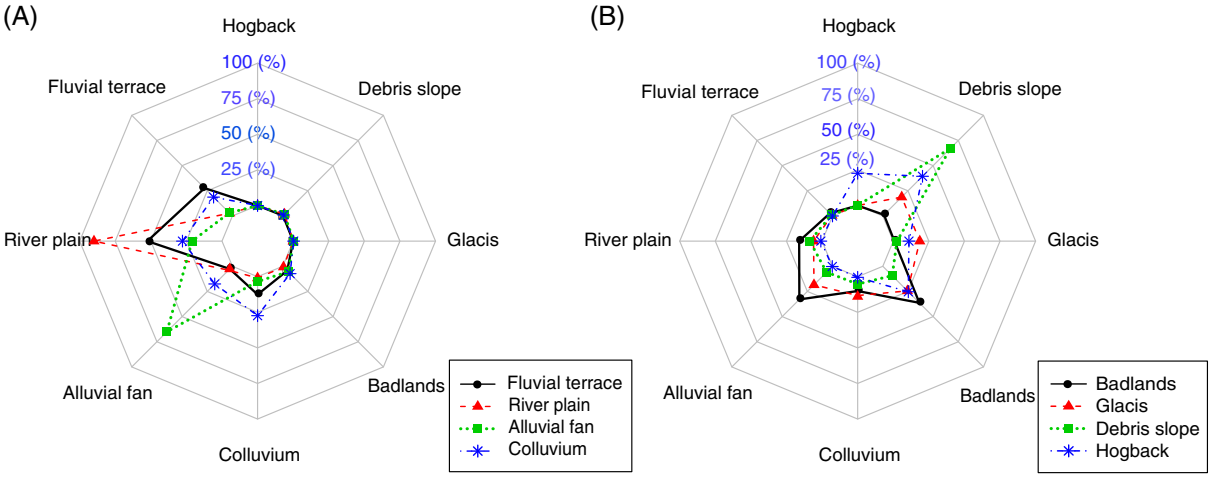

Fig. 9. Landforms observed at 10 cells downstream for cells in the fluvial environment (A) and in the hillslope environment (B). Each line shows the percentage of the landform classes (shown on the axis of the spider plots) observed 10 cells downstream from cells belonging to a particular landform.

classes that have similar characteristics to *hogback* and are more often present in the training image. The *hogback* was entirely misclassified as *debris slope* (Table 5).

Mapping accuracy is also relatively low for *glacis*, with Producer's Accuracy only 5%. *Glacis* is considerably misidentified as either *debris slope*, or, to a lesser extent, as *badlands* and *colluvium* (Table 5). The low mapping accuracy of *glacis* can be mainly explained by two factors. First, its characteristics overlap with other landform classes. With the chosen class boundaries, it is not possible to discretize the morphometric attributes to specifically correspond to the properties of *glacis* only (Fig. 8). This includes profile curvature, which is the key criterion to differentiate *glacis* from *debris slope* in field mapping, but does not enable discrimination between these two classes in automated mapping (Fig. 8C). Second, the training images contain a relatively low number of glacis cells compared to those of other units with overlapping characteristics, which affect the probability of the *glacis* with respect to other landforms. This results in an underestimation of *glacis* in the automated map and, consequently, in a low mapping accuracy of the *glacis* class. *Glacis* is only misclassified to landforms found in its adjacency (e.g. *debris slope*, *colluvium*, and *badlands*; Fig. 2).

Among the landforms in the fluvial environment, *fluvial terrace* is mapped with the lowest Producer's Accuracy of 20% (Table 5). *Fluvial terrace* is mainly misclassified as *alluvial fan* (42%) due to the overlapping properties of these two classes (Section 4.2). It is obvious that the mapping attributes used in this study are not sufficient to discriminate between *fluvial terrace* and *alluvial fan*. In field mapping, alluvial fans can easily be identified and separated from the fluvial terraces due to its prominent fan shape. However, attributes representing the shape and geometry of landforms are not used in this study due to the difficulties in translating and representing these attributes in a single grid cell as a DEM derivative. The low mapping accuracy of *fluvial terrace* may also be caused by low mapping quality of *river plain*, which is often observed at a direct downstream position of *fluvial terrace* (Fig. 9A). As the mapping criteria include landforms at downstream neighbors, errors in mapping the landforms at downslope locations may worsen the quality of mapping the upslope landforms. *River plain* is highly underestimated in the automated map and heavily misclassified to *alluvial fan* (Fig. 13, Table 5), causing omission errors in mapping *fluvial terrace*. Similarly to *glacis*, *fluvial terrace* and *river plain* are often misclassified to landforms in the fluvial environment, but rarely to landforms found in the hillslope environment.

4.4.3. Mapping quality relative to rule-based classification

MPS shows a better performance in creating the automated landform map compared to the rule-based classification. Using the rules defined in Fig. 15, the resulting automated map has 35.3% of correct cells (Fig. 16). Even though the rule-based map contains less noise and the landform units show a large spatial continuity with sizes comparable to those in the field map (i.e. average unit size difference of 1.9 km^2), the geometry of *glacis*, *badlands*, *colluvium*, and *alluvial fan*, is not correct. The rule-based technique produces units that are largely elongated in the direction of the elevation contours; however, in reality landform units extend along the slope direction or drainage network due to the slope aggradation or degradation processes that form the units (Fig. 5). This problem does not occur in the automated map generated by MPS. The rule-based technique largely overestimates the proportion of landforms that are not frequently observed in the field, i.e. *hogback*, *glacis*, and *fluvial terrace*, which results in an increased mapping accuracy of these landform classes compared to using MPS (Table 5). *Debris slope*, *alluvial fan*, and *badlands*, on the other hand, are considerably underrepresented in the rule-based map, while these landforms are quite ubiquitous in the Buëch valley. As a result, the mapping accuracy of these landform classes is low (Table 5). These findings clearly show that MPS outperforms the rule-based classification technique in landform mapping. The rule-based technique, however, has a superior capability to MPS in mapping *river plain*. This landform class can be mapped with correct shape and relatively high accuracy (80%), while its proportion is also comparable to the field map. Since *river plain* is specifically found at the lowest position in the landscape and its characteristics do not overlap other units, river plains can be mapped accurately even with a rule based on a single morphometric attribute (i.e. *HAND*, see Fig. 15).

4.5. Effect of training area on map quality

The size of the training area affects the mapping quality, irrespective of the criteria used in evaluating mapping accuracy. Here, we only discuss the results based on the percentage of correct cells (Fig. 17). It is shown that the average map quality in the mapping area (i.e. excluding the training area used in the base scenario) is highest for the scenario with the largest training area (i.e. the base mapping scenario). The decrease in mapping accuracy with training area size is related to the degree of mismatch between landform characteristics in the training area and the mapping area. Relations between topographical attributes and landform classes vary over the study site. This spatial non-stationarity is due to variations in geomorphological processes, to a large extent caused by variations in geology and hydrology. With a large training area, these variations are averaged out, resulting in a frequency tree that is representative for the entire region, and a high mapping accuracy. On the other hand, with a small training area, the frequency tree of the training area may not be representative for the mapping area, as it is derived from a small area that may have very specific landform characteristics. This bias results in a lower mapping accuracy. It is additionally shown that the mapping quality of individual training scenarios does significantly differ when the training area is small (Fig. 17), which is caused by the considerable differences in the frequency trees between small training areas.

It is found that the average mapping accuracy outside the training areas is only slightly lower when the size of the training areas is reduced from 10% to 7.5% of the total area. This reveals that in our study area, the optimal size of the training image is already reached at about 7.5% of the whole area. At this size, the training data set is already sufficiently large to establish a frequency database that is representative for mapping landforms in the remaining area.

The mapping quality is relatively high within the training areas (i.e. proportion of correct cells of 60–85%, and a kappa coefficient of 0.5–0.7). This can be regarded as the highest possible mapping accuracy because the information used to map landforms is completely contained in the training data set. Mapping errors inside the training images are solely caused by overlapping characteristics of landform classes. This source of error is intrinsic and unavoidable in the automated mapping, even when the landform characteristics of the training and mapping areas would be identical. The map quality within the training areas decreases with increasing size of the training images (Fig. 17). This can be explained by an increase in variability in the relations between landform classes and terrain attributes in the training data set, as certain landforms can be found under different attribute conditions over a large area. This non-stationarity results in more uncertainty in mapping.

5. Discussion and conclusion

5.1. General findings

In this study, we present an application of the multiple point geostatistics (MPS) technique to mapping the landforms, following the SNESIM approach and using a data set from the Buëch catchment, Southern France. The training data set consists of a field map of landforms and a DEM. In this approach, the data set is used to characterize the landforms, given (1) properties observed at the location itself and (2) properties in the neighborhood. The properties used in the study include four morphometric attributes at the cell of

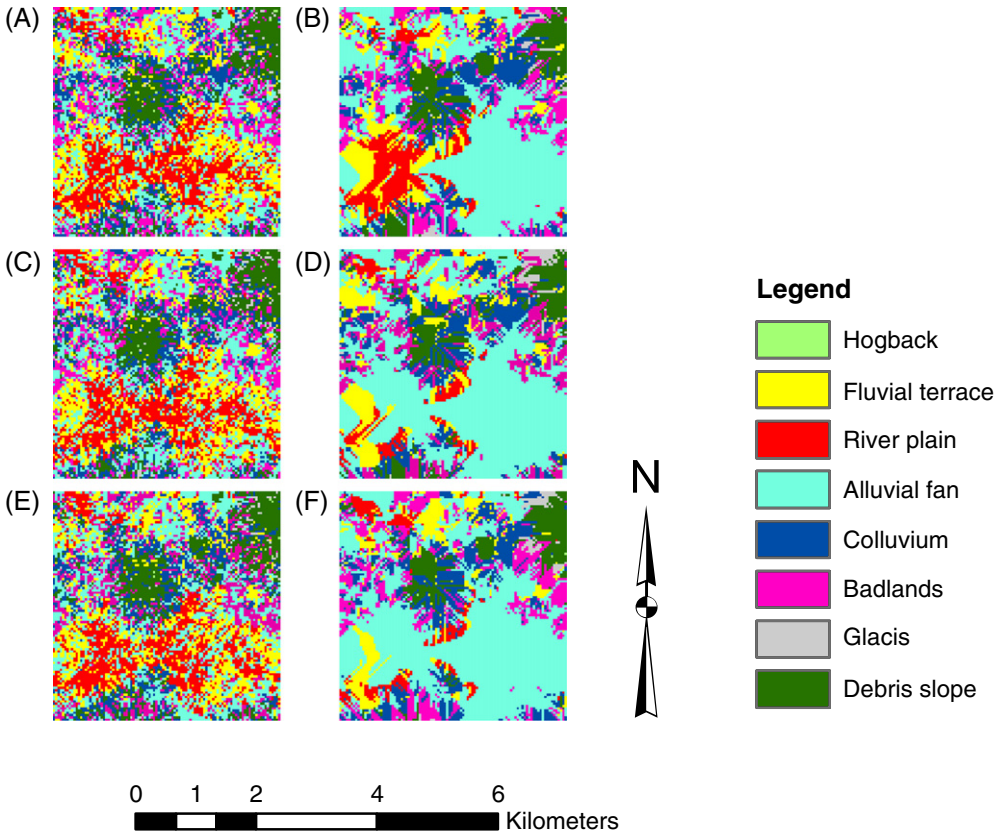

Fig. 10. Examples of map realizations as a result of different cell mapping orders, using the training images defined in the base scenario. Mapping the cells on a random basis (A, C, E) and mapping the cells on a systematic basis along the local drainage path in an upstream direction (B, D, F). Note that the map realizations are partly shown for the area within the box given in Fig. 12.

interest and two non-morphometric attributes at the neighboring cells.

The results show that the MPS technique is capable of reconstructing the general pattern of the landforms in the study area with a percentage of total correct cells of 51% and a kappa coefficient of 0.37, using training areas of 28 km^2, which represents 10% of the total mapping area. MPS outperforms a rule-based classification, which is essentially a one-point statistics technique, by 15% of overall cell accuracy, and regarding the capability of reproducing the shape of landform units and overall proportions of different landforms. With MPS, the mapping accuracy is largest at a high position in the landscape, where a single landform type, *debris slope* dominates. Quality of the automated map is somewhat lower in mid-slope and low-elevation areas as several landform types with overlapping characteristics can be found at these positions in the landscape. Mapping accuracy for landform classes considerably varies, with percentages of total correct cells ranging from 90% (i.e. *debris slope*) to 5% (i.e. *glacis*). With the exception of *debris slope*, landforms are generally better classified in the fluvial environment than in the hillslope environment. This is related to the statistical properties of the morphometric attributes characterizing the landforms. Landforms in the fluvial environment correspond to narrow ranges of attribute values with sharp boundaries, while the attribute values of a particular landform class often overlap with each other in the hillslope environment. It is also shown that mapping uncertainty is relatively large at cells near the boundaries of landform units, implying difficulties in identifying distinct boundaries between different landforms due to overlapping cell characteristics. The mapping quality decreases with a decrease in the size of the training area.

5.2. Evaluation of MPS for landform mapping

MPS has a number of advantages compared to other automated mapping techniques. The main advantage is that non-morphometric attributes at multiple point locations, i.e. landforms observed in the neighborhood, can be used to provide contextual information for mapping landforms at the location of interest. This contextual information is mostly used in field-geomorphological mapping, but often neglected in automated mapping techniques due to the incapability of two-point statistics in using these attributes to characterize landforms. MPS, thus, offers the opportunity to combine two classification paradigms using both geometric properties and the spatial pattern in geomorphological mapping. Also, using attributes in the neighborhood results in less noisy landform maps, because spatial correlation is taken into account. Furthermore, the MPS technique can be used to map landforms at any scale of interest because the landform classes to be mapped can be directly defined in the training data set. Finally, MPS allows probabilistic landform mapping, which enables the investigation and evaluation of mapping uncertainty at different locations and for different landforms. Map uncertainty is valuable information, both in academic and applied research, and is essential when landform maps are used as input to other analyses or models, for instance, when they are used as inputs to hydrological models for estimation of the spatial distribution of model parameters. Also, uncertainty information can be used to identify locations where additional field observations are required to improve the mapping quality.

The MPS technique has, however, a number of weaknesses in landform mapping. As categorical attribute values are used to

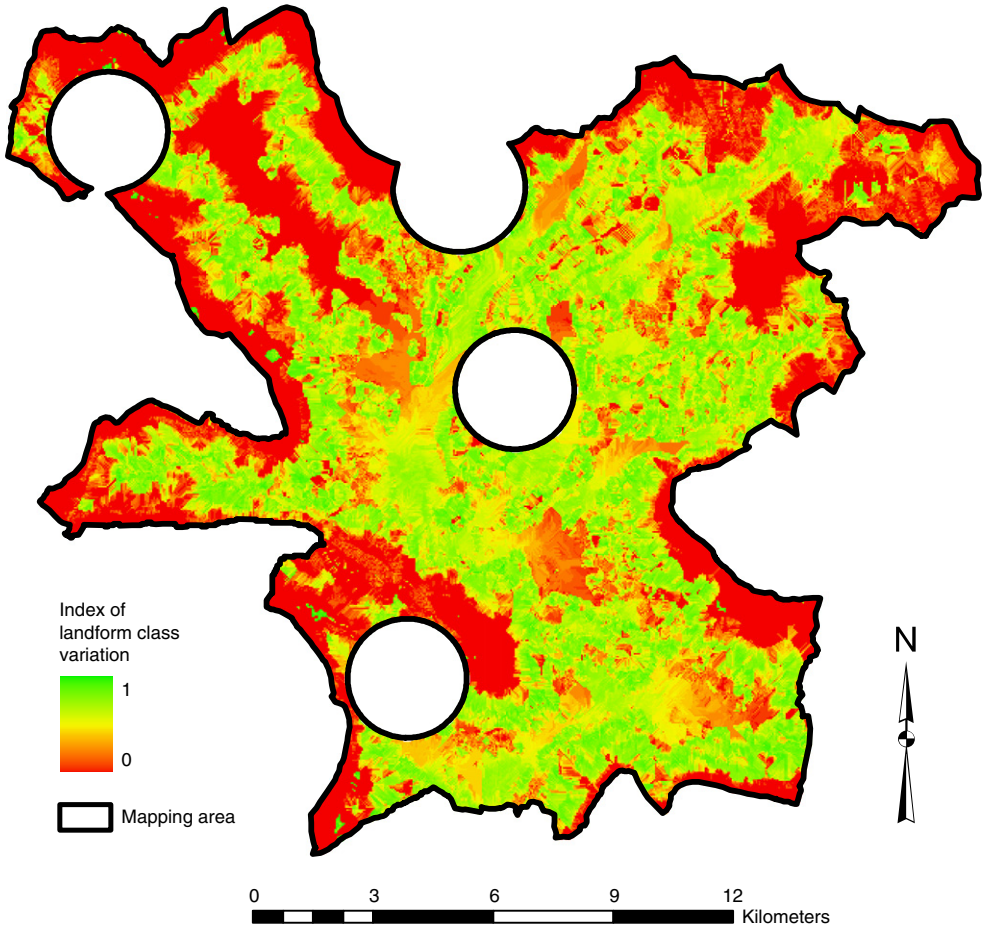

Fig. 11. Index of variation in landform classes mapped at certain cells (q_i, Eq. (2)). Note that the index does not represent the cell mapping accuracy.

characterize the occurrence of landforms, it is likely that landforms with overlapping characteristics are often related to the same set of attribute values. This hampers the discrimination between landform classes. Increasing the number of classes per attribute or using more attributes to improve the discrimination between landform classes may not be an appropriate solution. Indeed, the information used in characterizing and mapping landforms must be kept at a minimum to ensure a sufficient number of cell occurrences for each attribute pattern in the frequency database. Capability of the MPS technique in distinguishing different landforms is, therefore, limited by the amount of information tolerated to produce a reliable probability distribution. Another weakness of the MPS technique is the use of training data sets as an information source in mapping. Errors in the training data sets are intrinsically transferred to the automated map. These include errors in the field map of landforms itself, which are unavoidable in the automated map and cannot be evaluated, and errors caused by using training data sets that are not representative of landform characteristics in the mapping area. Also, the MPS technique tends to underestimate the landforms that are undersampled in the training images due to a low probability of unit occurrences, resulting from small counts in the frequency database, compared to those of other landforms with overlapping characteristics that are more often present in the training images. Finally, MPS is computationally intensive since the cells are sequentially mapped, and multiple map realizations are required. However, run time is not a big issue nowadays due to large computational capabilities of available computers.

5.3. Configuration of MPS for landform mapping

Results from this study suggest a promising future of the MPS technique in landform mapping. Successful application of MPS in landform mapping is, however, largely dependent on the configuration of the technique. Finding the appropriate configuration is not easy, as it depends on many factors, including the geomorphology at the study site. Thus, configuration of MPS should be optimized for individual cases based on expert knowledge and exploratory analysis of field data as was done in this study. Although a number of challenges exist for future research (see Section 5.4), we can provide from this study a number of recommendations for configuring MPS for mapping landforms.

5.3.1. Number of attributes and classes

First, during the training and mapping phases, the number of mapping attributes (e.g. DEM derivatives) and associated class numbers (e.g. slope classes) should not be too high. This is to ensure that sufficient replicates (i.e. number of cell counts) of attribute patterns occur in the training image, which is required for obtaining reliable statistics. In addition, we recommend to use a minimum number of cell counts during the mapping phase, as was also done by Liu (2006). We used a minimum of five, which could probably be used as a rule of thumb, although the optimal value will differ between studies, as it depends on the information used to create the search tree.

5.3.2. Order of visiting cells in mapping phase

The sequence of cell visits during mapping should not be random but organized to use previously-mapped cells, as conditioning data, as many

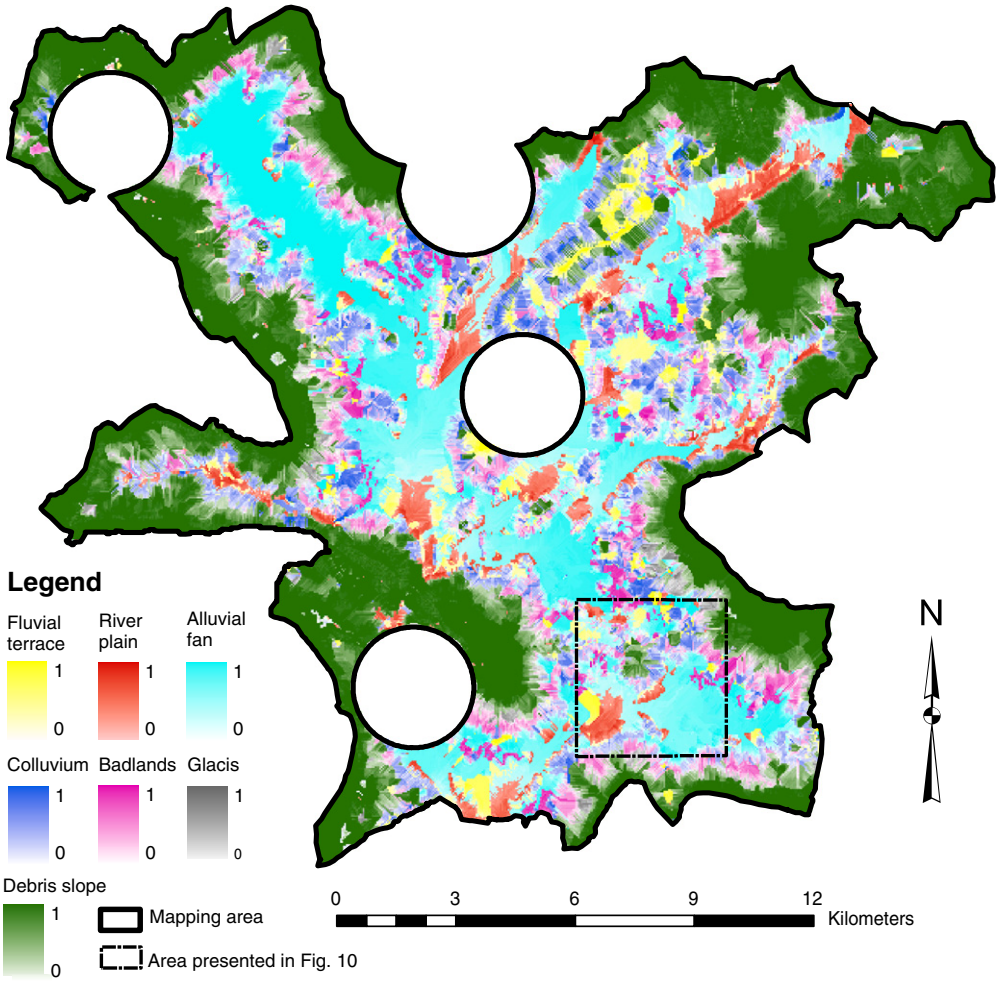

Fig. 12. Probability of landforms mapped in each cell, expressed as a shade of color for each landform class, for the base scenario. The box in the lower right indicates the area where the map realizations are shown in Fig. 10. Note that information about mapping accuracy is not given in this figure.

as possible. This is the case when visiting cells along the drainage network, because the mapping attributes include landforms at downstream cells. This issue is also addressed in Liu and Journel (2004) who developed an approach to structure the path of cell visit to maximize the number of conditioning data for simulation at non-visited cells.

5.3.3. Training image

The training image should contain multiple areas in the study site to avoid sampling bias. There is no strict guideline on the size of training image to be used (Hu and Chugunova, 2008); however, it should be sufficiently large to capture the spatial pattern and range of landform units (Caers and Zhang, 2004). We found an optimal training image size of 7.5–10% in the study area (20–28 km^2), which implies that the training image can be rather small to obtain a good mapping quality. Above this size, mapping quality does not significantly improve. This can be explained by an increase in variation in landform types observed under particular attribute conditions when the size of the training images becomes larger. Thus, the size of the training images must be chosen as to balance the variability within the training data set and the representativeness of the training data set for the mapping area.

5.3.4. Use of probabilistic information

We do not recommend deterministic mapping based on the maximum probability of landform class per attribute. In deterministic mapping, the landform most frequently observed per attribute pattern in the training image will always be mapped, while other landforms with overlapping characteristics that are less present in the training images will be totally neglected. This results in an overrepresentation in the automated map of landforms that are most dominating in the training image. Therefore, it is beneficial to follow a Monte Carlo approach, requiring at least 30 realizations for consistent results.

5.4. Future perspectives

A number of strategies need to be explored to improve the quality of the automated maps in future studies. Morphometric attributes that are not capable of discriminating between landform classes (e.g. profile curvature) should most likely be dropped out and replaced by non-morphometric attributes, which include landforms at a larger number of neighboring locations (i.e. landforms at longer distances than 10 cells downstream), and attributes related to vegetation, soil, or land cover, possibly retrieved through remote sensing. This information enables more detailed landform classification; for instance, badlands with different stages of development, or fluvial terraces with different formation ages. With the use of more neighborhood attributes, a multi-grid simulation approach is required to prevent attribute patterns with a too small number of replicates and to reduce the size of frequency tree (Hu and Chugunova, 2008).

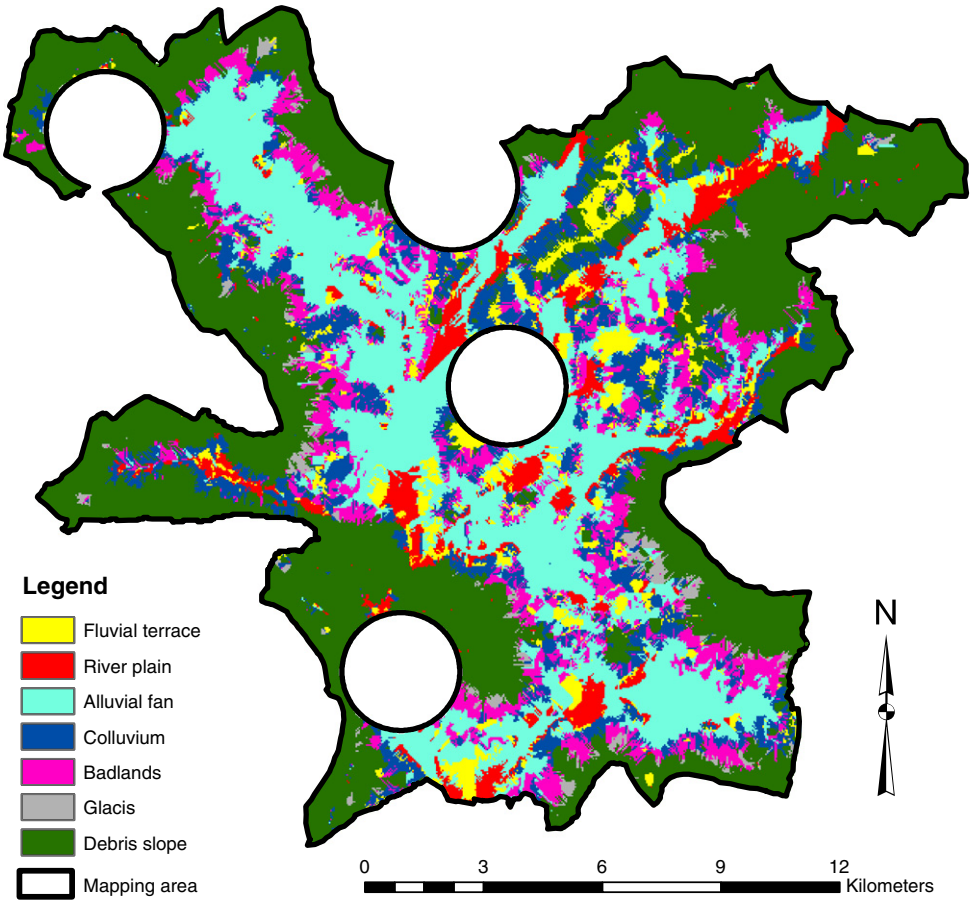

Fig. 13. Final geomorphological map using training areas defined in the base scenario.

Mapping quality could also be improved by using hard conditioning data such as landforms mapped in the field at multiple locations in the study area, or automatically extracted landform features with extreme morphometric characteristics (e.g. Miliaresis and Argialas, 2000; Stout and Belmont, 2013). Note that this option requires a very large number of conditioning locations since the cells at further distances might not be influenced by this hard conditioning data (Liu, 2006). Quality of the automated map can be also improved by improving the quality of the field geomorphological map used as a training data set. Also, high-resolution topographical data such as LIDAR DTMs (Anders et al., 2011), ASTER

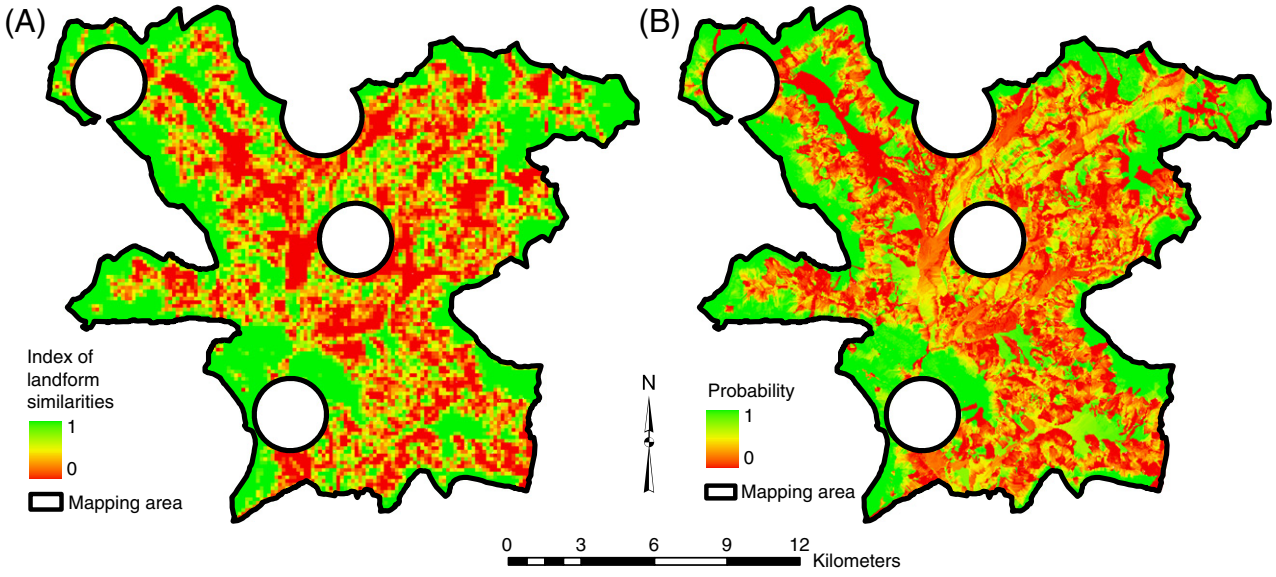

Fig. 14. Quality of the automated map in the base scenario. A) Index of cell similarities (i.e. landform classes) between the automated map in the base scenario and the field map, evaluated over a template of 4 × 4 pixels (s_i, Eq. (4)); 1 = similar, 0 = dissimilar. B) Probability of correct cell mapping.

Table 5
Confusion matrix showing the number of cells in the automated map of the base scenario (column), derived from MPS, classified to landform classes in the field map (row). Mapping accuracy of the automated map from the rule-based classification is shown in the last column.

	Landform classes	Automated map									Producer's Accuracy, MPS (%)	Producer's Accuracy, rule-based (%)
		Hogback	Fluvial terrace	River plain	Alluvial fan	Colluvium	Badlands	Glacis	Debris slope	Total cells		
Field map	Hogback	0	0	0	0	0	0	0	420	420	0	57.1
	Fluvial terrace	0	2709	1485	5517	1826	949	7	637	13,130	20.6	42.4
	River plain	0	1016	5185	11,820	604	525	6	817	19,973	26.0	81.1
	Alluvial fan	0	1883	1289	14,338	2391	3959	172	1026	25,058	57.2	18.4
	Colluvium	0	1689	598	3367	5222	2665	174	2801	16,516	31.6	30.7
	Badlands	0	1343	464	5830	6838	6609	1068	8228	30,380	21.8	12.3
	Glacis	0	288	68	488	1063	1046	444	4836	8233	5.4	22.6
	Debris slope	0	437	756	333	2346	1727	1215	55,676	62,490	89.1	39.9
	Total cells	0	9378	9854	41,734	20,307	17,508	3088	74,469	176,338	Overall accuracy (%)	
	User's accuracy (%)	0	28.9	52.6	34.4	25.7	37.7	14.3	74.8		51.2	35.3

GDEM (Tachikawa et al., 2011), and HRSC-A (Otto et al., 2007), can be used as base information to improve mapping quality of small-scale landform units (e.g. slopes with mass movement and hogbacks).

Future studies also need to use an improved simulation procedure. Bayesian updating and servo-system correction can be implemented to constrain the statistics of the simulated map to the global statistics of the mapping area (Liu, 2006). If landform characteristics exhibit a strong spatial inconsistency (i.e. non-stationarity), the entire mapping area can be dissected into sub-regions of relatively uniform geomorphological characteristics, where mapping the landforms can be done on a separate basis using different training data sets (e.g. de Vries et al., 2009). It would also be worthwhile to apply other MPS approaches in geomorphological mapping. Recent MPS algorithms (e.g. Zhang et al., 2006; Chugunova and Hu, 2008; Mariethoz et al., 2010; Straubhaar et al., 2011) allow using continuous data as auxiliary variables to control the position of the pattern; and classification is made based on pattern matching. These techniques are computationally fast as they avoid using the search trees to store the statistics from the training images and allow a parallel simulation within the same mapping domain. These algorithms are, therefore, suitable to deal with non-stationary images and simulation domain (Straubhaar et al., 2011). It might also be important to revise the procedure in deriving the final landform map, in order to reduce the possible overestimation of landform classes that are oversampled in the training image (Soares, 1992).

In addition to improving mapping quality, it is also important to prove the applicability of the automated maps generated by the MPS technique, for example, in landscape planning or hydrological prediction. Delineation of the response units used in the semi-distributed hydrological modeling is in many studies based on landform components and geomorphological features as they generally represent areas with hydrological similarities due to internal homogeneity of morphometric and physical properties (e.g. Tilch et al., 2002; Güntner and Bronstert, 2004; Uhlenbrook et al., 2004; Pluntke et al., 2013; Vannametee et al., 2013). Thus, an automated landform map can be incorporated into a hydrological modeling framework to provide information on the model units and model parameterization (e.g. Khan et al., 2013). In this way, benefits and values of automated landform mapping, including the performance of the MPS technique, can be evaluated from a practical perspective. This

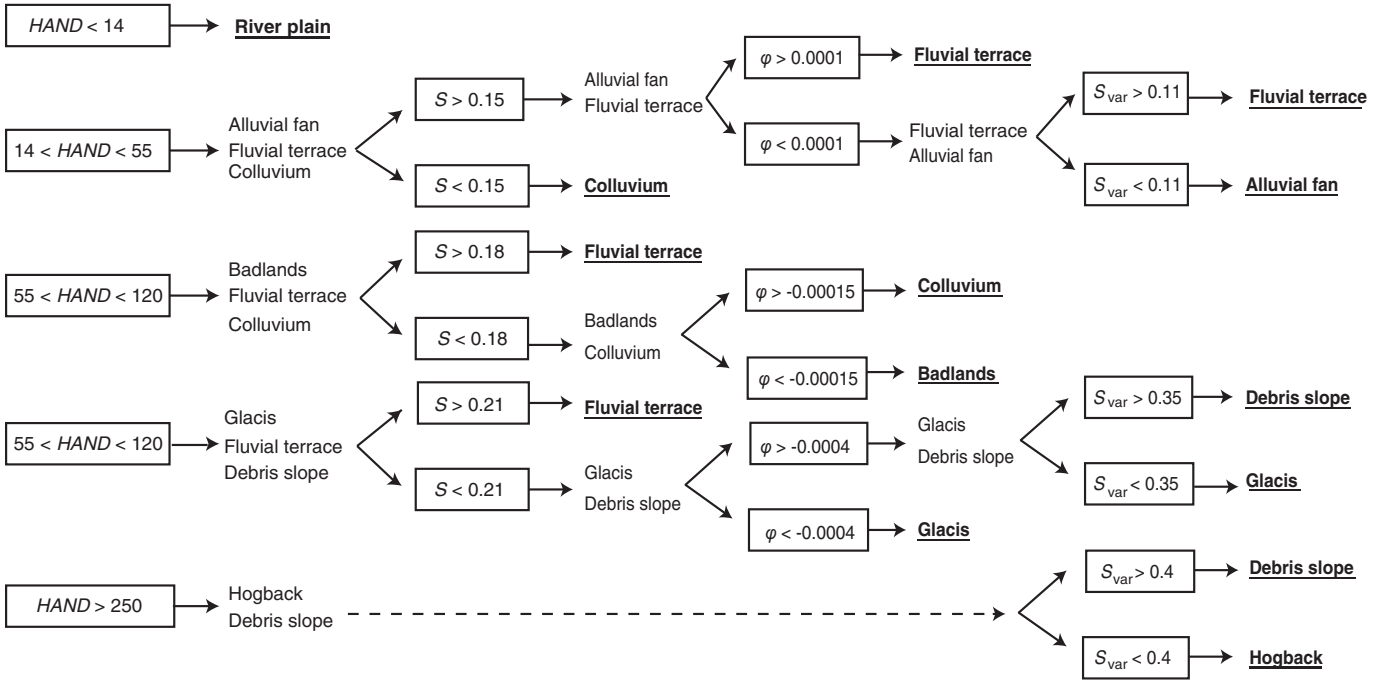

Fig. 15. Landform classification rules derived from the analysis of information in training images in the base scenario. Each rule represents a single landform class (bold and underlined). *HAND* = height above the nearest drainage; S = slope gradient; φ = profile curvature; S_{var} = slope variability.

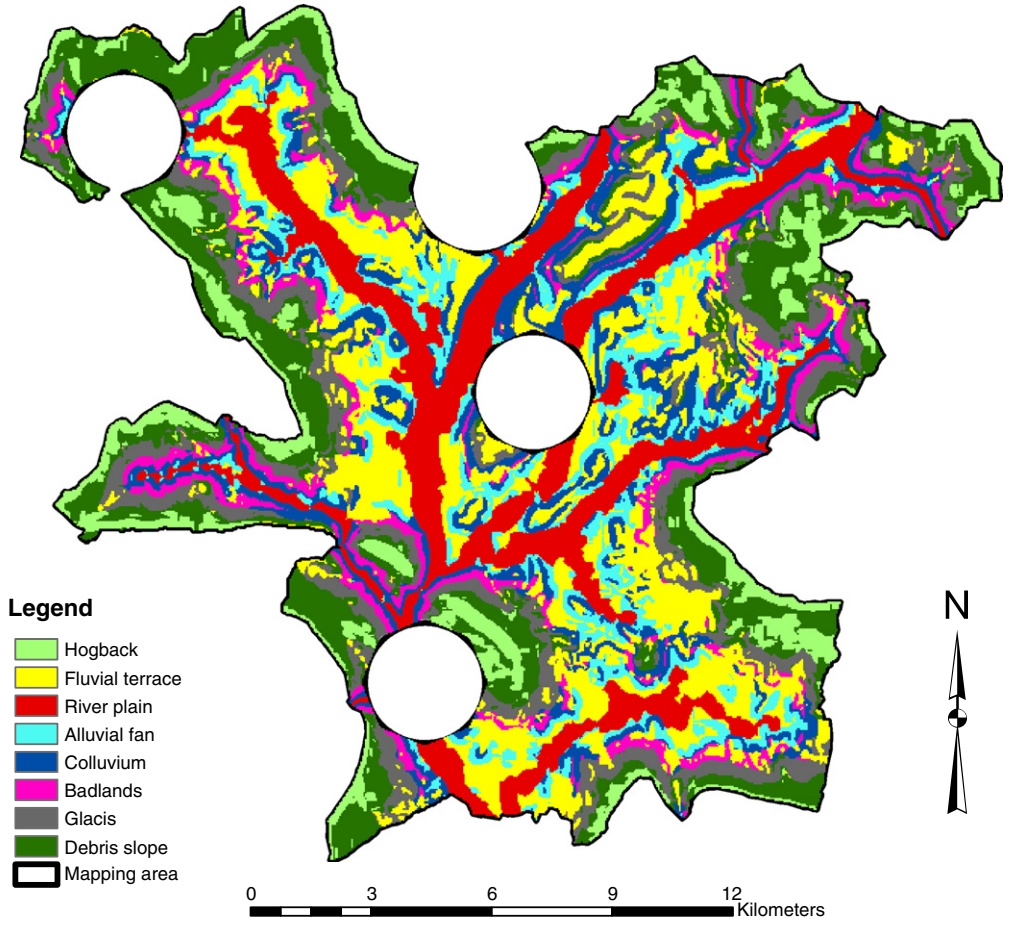

Fig. 16. Automated geomorphological map derived from the classification rules in Fig. 15.

will, in turn, deliver useful information for an improvement of the MPS technique in mapping landforms to serve a specific application.

Acknowledgments

This research is supported by the Anadamahidol scholarship, under the royal patronage of the King of Thailand, granted to Ekkamol Vannametee. The authors would like to thank Cees Wesseling for programming the SNESIM algorithm in the Python framework used in this paper. The editor, Prof. Takashi Oguchi, and two anonymous reviewers are also thanked for their constructive comments for improving the original manuscript.

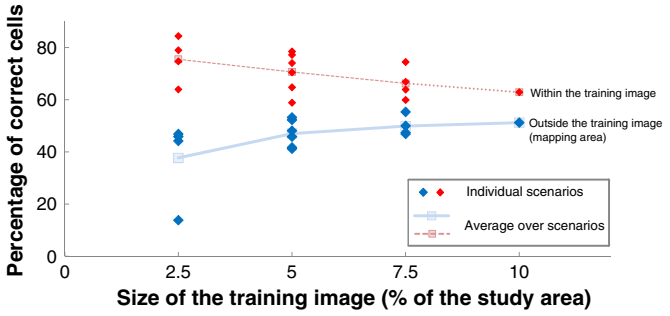

Fig. 17. Percentage of correct cells versus the size of the training images.

References

Adediran, A.O., Parcharidis, I., Poscolieri, M., Pavlopoulos, K., 2004. Computer-assisted discrimination of morphological units on north-central Crete (Greece) by applying multivariate statistics to local relief gradients. Geomorphology 58, 357–370.
Anders, N.S., Seijmonsbergen, A.C., Bouten, W., 2011. Segmentation optimization and stratified object-based analysis for semi-automated geomorphological mapping. Remote Sens. Environ. 115, 2976–2985.
Arattano, M., Conte, R., Franzi, L., Giordan, D., Lazzari, A., Luino, F., 2010. Risk management on an alluvial fan: a case study of the 2008 debris-flow event at Villar Pellice (Piedmont, N–W Italy). Nat. Hazards Earth Syst. Sci. 10, 999–1008.
Atkinson, P., Jiskoot, H., Massari, R., Murray, T., 1998. Generalized linear modelling in geomorphology. Earth Surf. Process. Landforms 23, 1185–1195.
Battiau-Queney, Y., 2005. French Alps and Alpine forelands. In: Koster, E.A. (Ed.), The Physical Geography of Western Europe. Oxford University Press, pp. 267–285.
Benger, S.N., 2003. Remote sensing of vegetation surrogates for regolith landform mapping. IGARSS 2003. 2003 IEEE International Geoscience and Remote Sensing Symposium. Proceedings (IEEE Cat. No. 03CH37477). IEEE, pp. 3320–3322.
Bishop, M.P., James, L.A., Shroder, J.F., Walsh, S.J., 2012. Geospatial technologies and digital geomorphological mapping: concepts, issues and research. Geomorphology 137, 5–26.
Blanchard, R., 1921. The natural regions of the French Alps. Geogr. Rev. 11, 31–49.
Bolongaro-Crevenna, A., Torres-Rodríguez, V., Sorani, V., Frame, D., Arturo Ortiz, M., 2005. Geomorphometric analysis for characterizing landforms in Morelos State, Mexico. Geomorphology 67, 407–422.
Boucher, A., 2007. Downscaling of Satellite Remote Sensing Data: Application to Land Cover Mapping. Ph.D. thesis Stanford University, USA.
Brocard, G.Y., van der Beek, P.A., 2006. Influence of incision rate, rock strength, and bedload supply on bedrock river gradients and valley-flat widths: field-based evidence and calibrations from western Alpine rivers (southeast France). In: Willett, S. D., Hovius, N., Brandon, M.T., Fisher, D.M. (Eds.), Tectonics, Climate, and Landscape Evolution: Geological Society of America Special Paper 398, Penrose Conference Series, pp. 101–126.
Brocard, G.Y., van der Beek, P.A., Bourlès, D.L., Siame, L.L., Mugnier, J.-L., 2003. Long-term fluvial incision rates and postglacial river relaxation time in the French Western Alps from 10Be dating of alluvial terraces with assessment of inheritance, soil development and wind ablation effects. Earth Planet. Sci. Lett. 209, 197–214.
Bue, B.D., Stepinski, T.F., 2006. Automated classification of landforms on Mars. Comput. Geosci. 32, 604–614.

Burl, M.C., Fayyad, U.M., Perona, P., Smyth, P., Burl, M.P., 1994. Automating the hunt for volcanoes on Venus. Proceedings of IEEE Conference on Computer Vision and Pattern Recognition CVPR-94. IEEE Computer Society Press, pp. 302–309.
Burrough, P.A., McDonnell, R.A., 2004. Principles of Geographical Information Systems, 5th ed. Oxford University Press, New York.
Burrough, P.A., van Gaans, P.F.M., MacMillan, R.A., 2000. High-resolution landform classification using fuzzy-means. Fuzzy Sets Syst. 113, 37–52.
Caers, J., 2001. Geostatistical reservoir modelling using statistical pattern recognition. J. Pet. Sci. Eng. 29, 177–188.
Caers, J., Zhang, T., 2004. Multiple-point geostatistics: a quantitative vehicle for integrating geologic analogs into multiple reservoir models. In: Gramer, M., Harris, P.M., Eberli, G.P. (Eds.), Integration of Outcrop and Modern Analogs in Reservoir Modeling. American Association of Petroleum Geologist Memoir, pp. 383–394.
Chartin, C., Bourennane, H., Salvador-Blanes, S., Hinschberger, F., Macaire, J.-J., 2011. Classification and mapping of anthropogenic landforms on cultivated hillslopes using DEMs and soil thickness data — example from the SW Parisian Basin, France. Geomorphology 135, 8–20.
Chugunova, T.L., Hu, L.Y., 2008. Multiple-point simulations constrained by continuous auxiliary data. Math. Geosci. 40, 133–146.
Comunian, A., Renard, P., Straubhaar, J., Bayer, P., 2011. Three-dimensional high resolution fluvio-glacial aquifer analog — part 2: geostatistical modeling. J. Hydrol. 405, 10–23.
De Vries, L.M., Carrera, J., Falivene, O., Gratacós, O., Slooten, L.J., 2009. Application of multiple point geostatistics to non-stationary images. Math. Geosci. 41, 29–42.
Dehn, M., Gärtner, H., Dikau, R., 2001. Principles of semantic modeling of landform structures. Comput. Geosci. 27, 1005–1010.
Descroix, L., Gautier, E., 2002. Water erosion in the southern French alps: climatic and human mechanisms. Catena 50, 53–85.
Descroix, L., Olivry, J.C., 2002. Spatial and temporal factors of erosion by water of black marls in the badlands of the French southern Alps. Hydrol. Sci. 47, 227–242.
Dikau, R., Brabb, E., Mark, R.K., Pike, R.J., 1995. Morphometric landform analysis of New Mexico. Z. Geomorphol. Suppl. 109–126.
Drăguţ, L., Blaschke, T., 2006. Automated classification of landform elements using object-based image analysis. Geomorphology 81, 330–344.
Dramis, F., Guida, D., Cestari, A., 2011. Nature and aims of geomorphological mapping. In: Smith, M.J., Paron, P., Griffiths, J.S. (Eds.), Geomorphological Mapping. Methods and Applications. Elsevier B.V., pp. 39–73.
Dumas, B., Guérémy, P., Lecompte, M., Lhénaff, R., Raffy, J., 1987. Mouvements de terrain et érosion hydrique dans les Baronnies Méridionales: méthod d'étude et premiers résultats. Travaux de l'Institut de Géographie de Reims, pp. 68–93.
Dymond, J.R., Derose, R.C., Harmsworth, G.R., 1995. Automated mapping of land components from digital elevation data. Earth Surf. Process. Landforms 20, 131–137.
Etzelmüller, B., Romstad, B., Fjellanger, J., 2007. Automatic regional classification of topography in Norway. Nor. J. Geol. 87, 167–180.
Evans, I.S., 2012. Geomorphometry and landform mapping: what is a landform? Geomorphology 137, 94–106.
Evans, I.S., Cox, N.J., 1999. Relations between land surface properties: altitude, slope and curvature. In: Hergarten, S., Neugebauer, H.J. (Eds.), Process Modelling and Landform Evolution, Lecture Notes in Earth Sciences. Springer-Verlag, Berlin/Heidelberg, pp. 13–45.
Feyen, L., Caers, J., 2005. Multiple-point geostatistics: a powerful tool to improve groundwater flow and transport predictions in multi-modal formations. Geostat. Environ. Appl. 2005, 197–208.
Florinsky, I.V., 2008. Global morphometric maps of Mars, Venus, and the Moon. In: Moore, A., Drecki, I. (Eds.), Geospatial Vision: New Dimensions in Cartography (Lecture Notes in Geoinformation and Cartography). Springer, Berlin, pp. 171–192.
Gharari, S., Hrachowitz, M., Fenicia, F., Savenije, H.H.G., 2011. Hydrological landscape classification: investigating the performance of HAND based landscape classifications in a central European meso-scale catchment. Hydrol. Earth Syst. Sci. 15, 3275–3291.
Gibbs, J.P., Poston, D.L., 1975. The division of labor: conceptualization and related measures. Soc. Forces 53, 468–476.
Guardiano, F., Srivastava, R.M., 1993. Multivariate geostatistics: beyond bivariate moments. In: Soares, A. (Ed.), Geostatistics Troia. Kluwer, Dordrecht, pp. 133–144.
Güntner, A., Bronstert, A., 2004. Representation of landscape variability and lateral redistribution processes for large-scale hydrological modelling in semi-arid areas. J. Hydrol. 297, 136–161.
Hagen-Zanker, A., 2006. Map comparison methods that simultaneously address overlap and structure. J. Geogr. Syst. 8, 165–185.
Hammond, E.H., 1964. Analysis of properties in land form geography: an application to board-scale land form mapping. Ann. Assoc. Am. Geogr. 54, 11–19.
Hengl, T., Rossiter, D.G., 2003. Supervised landform classification to enhance and replace photo-interpretation in semi-detailed soil survey. Soil Sci. Soc. Am. J. 67, 1810–1821.
Ho, L.T.K., Yamaguchi, Y., Umitsu, M., 2012. Rule-based landform classification by combining multi-spectral/temporal satellite data and the SRTM DEM. Int. J. Geoinformatics 8, 27–38.
Ho, L.T.K., Yamaguchi, Y., Umitsu, M., 2013. Delineation of small-scale landforms relative to flood inundation in the western Red River delta, northern Vietnam using remotely sensed data. Nat. Hazards 69, 905–917.
Honarkhah, M., 2011. Stochastic Simulation of Patterns Using Distance-based Pattern Modeling. Ph.D. thesis Stanford University, USA.
Hu, L.Y., Chugunova, T., 2008. Multiple-point geostatistics for modeling subsurface heterogeneity: a comprehensive review. Water Resour. Res. 44. http://dx.doi.org/10.1029/2008WR006993.
Huysmans, M., Dassargues, A., 2009. Application of multiple-point geostatistics on modelling groundwater flow and transport in a cross-bedded aquifer (Belgium). Hydrogeol. J. 17, 1901–1911.
Irvin, B.J., Ventura, S.J., Slater, B.K., 1997. Fuzzy and isodata classification of landform elements from digital terrain data in Pleasant Valley, Wisconsin. Geoderma 77, 137–154.
Jain, A., Suresh, K., Thakore, D., Patel, N., 2013. Automatic crater detection on Lunar surface. Int. J. Innov. Res. Sci. Eng. Technol. 2, 1448–1453.
Jordan, G., 2003. Morphometric analysis and tectonic interpretation of digital terrain data: a case study. Earth Surf. Process. Landforms 28, 807–822.
Karssenberg, D., de Jong, K., van der Kwast, J., 2007. Modelling landscape dynamics with Python. Int. J. Geogr. Inf. Sci. 21, 483–495.
Khan, U., Tuteja, N.K., Sharma, A., 2013. Delineating hydrologic response units in large upland catchments and its evaluation using soil moisture simulations. Environ. Model. Softw. 46, 142–154.
Klingseisen, B., Metternicht, G., Paulus, G., 2008. Geomorphometric landscape analysis using a semi-automated GIS-approach. Environ. Model. Softw. 23, 109–121.
Knudby, C., Carrera, J., 2005. On the relationship between indicators of geostatistical, flow and transport connectivity. Adv. Water Resour. 28, 405–421.
Lillesand, T., Kiefer, R.W., Chipman, J., 2004. Remote Sensing and Image Interpretation, 5th ed. John & Wiley and Sons, New York.
Liu, Y., 2006. Using the SNESIM program for multiple-point statistical simulation. Comput. Geosci. 32, 1544–1563.
Liu, Y., Journel, A., 2004. Improving sequential simulation with a structured path guided by information content. Math. Geol. 36, 945–964.
Luoto, M., Hjort, J., 2005. Evaluation of current statistical approaches for predictive geomorphological mapping. Geomorphology 67, 299–315.
MacMillan, R.A., Pettapiece, W.W., Nolan, S.C., Goddard, T.W., 2000. A generic procedure for automatically segmenting landforms into landform elements using DEMs, heuristic rules and fuzzy logic. Fuzzy Sets Syst. 113, 81–109.
MacMillan, R.A., Jones, R.K., McNabb, D.H., 2004. Defining a hierarchy of spatial entities for environmental analysis and modeling using digital elevation models (DEMs). Comput. Environ. Urban. Syst. 28, 175–200.
Mariethoz, G., Lefebvre, S., 2014. Bridges between multiple-point geostatistics and texture synthesis: review and guidelines for future research. Comput. Geosci. 66, 66–80.
Mariethoz, G., Renard, P., Straubhaar, J., 2010. The Direct Sampling method to perform multiple-point geostatistical simulations. Water Resour. Res. 46. http://dx.doi.org/10.1029/2008WR007621.
Matsuura, T., Aniya, M., 2012. Automated segmentation of hillslope profiles across ridges and valleys using a digital elevation model. Geomorphology 177–178, 167–177.
Meerschman, E., van Meirvenne, M., van de Vijver, E., de Smedt, P., Islam, M.M., Saey, T., 2013. Mapping complex soil patterns with multiple-point geostatistics. Eur. J. Soil Sci. 64, 183–191.
Miliaresis, G.C., Argialas, D.P., 2000. Extraction and delineation of alluvial fans from digital elevation models and Landsat thematic mapper images. Photogramm. Eng. Remote Sens. 66, 1093–1101.
Minár, J., Evans, I.S., 2008. Elementary forms for land surface segmentation: the theoretical basis of terrain analysis and geomorphological mapping. Geomorphology 95, 236–259.
Miramont, C., Sivan, O., Rosique, T., Edouard, J.L., Jorda, M., 2000. Subfossil tree deposits in the middle Durance (southern Alps, France): environmental changes from Allerod to Atlantic. Radiocarbon 42, 423–435.
Nobre, A.D., Cuartas, L.A., Hodnett, M., Rennó, C.D., Rodrigues, G., Silveira, A., Waterloo, M., Saleska, S., 2011. Height Above the Nearest Drainage — a hydrologically relevant new terrain model. J. Hydrol. 404, 13–29.
Otto, J.C., Dikau, R., 2004. Geomorphologic system analysis of a high mountain valley in the Swiss Alps. Z. Geomorphol. 48, 323–341.
Otto, J.-C., Kleinod, K., Konig, O., Krautblatter, M., Nyenhuis, M., Roer, I., Schneider, M., Schreiner, B., Dikau, R., 2007. HRSC-A data: a new high-resolution data set with multipurpose applications in physical geography. Prog. Phys. Geogr. 31, 179–197.
Pluntke, T., Bernhofer, C., Schanze, J., Burmeister, C., Schwärzel, K., Kh, F., Trümper, J., Fischer, S., Kovalchuk, I., Nabyvanets, Y., Snizhko, S., Vyshnevskyy, V., Kruhlov, I., Tarasiuk, M., Shevchenko, O., Obodovskiy, A., Rozlach, Z., Konovalenko, O., Mkrtchian, O., Shuber, P., 2013. Handbook: ideas, data and methods for the setup of the water balance atlas of the Western Ukraine. 90 p. Retrieved from http://tu-dresden.de/die_tu_dresden/fakultaeten/fakultaet_forst_geo_und_hydrowissenschaften/fachrichtung_wasserwesen/ifhm/meteorologie/forschung/projekte/projekt_wtz/Handbook-Water-Balance-Atlas.pdf.
Pontius, R.G., Huffaker, D., Denman, K., 2004. Useful techniques of validation for spatially explicit land-change models. Ecol. Model. 179, 445–461.
Rennó, C.D., Nobre, A.D., Cuartas, L.A., Soares, J.V., Hodnett, M.G., Tomasella, J., Waterloo, M.J., 2008. HAND, a new terrain descriptor using SRTM-DEM: mapping terra-firme rainforest environments in Amazonia. Remote Sens. Environ. 112, 3469–3481.
Reuter, H.I., Wendroth, O., Kersebaum, K.C., 2006. Optimisation of relief classification for different levels of generalisation. Geomorphology 77, 79–89.
Rezaee, H., Asghari, O., Koneshloo, M., 2011. The application of multiple-point geostatistics in the modeling of dike; a case study of Sungun Porphyry Copper, Iran. pp. 1–12.
Ridefelt, H., Etzelmüller, B., Boelhouwers, J., 2010. Spatial analysis of solifluction landforms and process rates in the Abisko Mountains, northern Sweden. Permafr. Periglac. Process. 21, 241–255.
Romstad, B., 2001. Improving relief classification with contextual merging. In: Bjorke, J.T., Tveite, H. (Eds.), 8th Scandinavian Research Conference on Geographical Information Science, ScanGIS'2001; Conference Proceedings. Ås, Norway, pp. 3–14.
Ruszkiczay-Rüdiger, Z., Fodor, L., Horváth, E., Telbisz, T., 2009. Discrimination of fluvial, eolian and neotectonic features in a low hilly landscape: a DEM-based morphotectonic analysis in the Central Pannonian Basin, Hungary. Geomorphology 104, 203–217.
Schneevoigt, N.J., van der Linden, S., Thamm, H.-P., Schrott, L., 2008. Detecting Alpine landforms from remotely sensed imagery. A pilot study in the Bavarian Alps. Geomorphology 93, 104–119.
Seijmonsbergen, H., 2008. Digital geomorphological information for alpine hazard studies using laser altimetry data and GIS: with an example from Vorarlberg, Austria. In:

Mikoś, M., Hübel, J., Koboltschnig, G. (Eds.), Interpraevent: 26–30 May 2008, Dornbirn, Vorarlberg, Austria: Conference Proceedings, vol. 2. Kreiner Druck, Villach, pp. 395–406.
Seijmonsbergen, A.C., Hengl, T., Anders, N.S., 2011. Semi-automated identification and extraction of geomorphological features using digital elevation data. In: Smith, M.J., Paron, P., Griffiths, J. (Eds.), Geomorphological Mapping: Methods and Applications. Elsevier, Amsterdam, pp. 297–335.
Skidmore, A.K., 1989. A comparison of techniques for calculating gradient and aspect from a gridded digital elevation model. Int. J. Geogr. Inf. Syst. 3, 323–334.
Soares, A., 1992. Geostatistical estimation of multi-phase structures. Math. Geol. 24, 149–160.
Speight, J.G., 1990. Landform. In: McDonald, R.C., Isbell, R.F., Speight, J.G., Walker, J., Hopkins, M.S. (Eds.), Australian Soil and Land Survey Field Handbook. Inkarta Press, Melbourne, pp. 9–57.
Stepinski, T., Vilalta, R., 2005. Digital topography models for Martian surfaces. IEEE Geosci. Remote Sens. Lett. 2, 260–264.
Stepinski, T., Vilalta, R., Ghosh, S., 2007. Machine learning tools for automatic mapping of Martian landforms. IEEE Intell. Syst. 22, 100–106.
Stout, J.C., Belmont, P., 2013. TerEx Toolbox for semi-automated selection of fluvial terrace and floodplain features from lidar. Earth Surf. Process. Landforms 39, 569–580.
Straubhaar, J., Renard, P., Mariethoz, G., Froidevaux, R., Besson, O., 2011. An improved parallel multiple-point algorithm using a list approach. Math. Geosci. 43, 305–328.
Strebelle, S., 2002. Conditional simulation of complex geological structures using multiple-point statistics. 1 (34), 1–21.
Sulebak, J.R., Etzelmüller, B., Sollid, J.L., 1997. Landscape regionalization by automatic classification of landform elements. Nor. Geogr. Tidsskr. Nor. J. Geogr. 51, 35–45.
Tachikawa, T., Hato, M., Kaku, M., Iwasaki, A., 2011. The characteristics of ASTER GDEM version 2. International Geoscience and Remote Sensing Symposium. Vancouver, Canada, p. 4.
Tang, Y., Atkinson, P.M., Wardrop, N.A., Zhang, J., 2013. Multiple-point geostatistical simulation for post-processing a remotely sensed land cover classification. Spat. Stat. 5, 69–84.
Thuiller, W., Araújo, M.B., Lavorel, S., 2003. Generalized models vs. classification tree analysis: predicting spatial distributions of plant species at different scales. J. Veg. Sci. 14, 669.
Tilch, N., Uhlenbrook, S., Leibundgut, C., 2002. Regionalisierungsverfahren zur Ausweisung von Hydrotopen in von periglazialem Hangschutt geprägten Gebieten. Grundwasser 7, 206–216.
Trevisani, S., Cavalli, M., Marchi, L., 2009. Variogram maps from LiDAR data as fingerprints of surface morphology on scree slopes. Nat. Hazards Earth Syst. Sci. 9, 129–133.
Uhlenbrook, S., Roser, S., Tilch, N., 2004. Hydrological process representation at the meso-scale: the potential of a distributed, conceptual catchment model. J. Hydrol. 291, 278–296.
Van Asselen, S., Seijmonsbergen, A.C., 2006. Expert-driven semi-automated geomorphological mapping for a mountainous area using a laser DTM. Geomorphology 78, 309–320.
Van Niekerk, A., 2010. A comparison of land unit delineation techniques for land evaluation in the Western Cape, South Africa. Land Use Policy 27, 937–945.
Vannametee, E., Karssenberg, D., Hendriks, M.R., Bierkens, M.F.P., 2013. Hortonian runoff closure relations for geomorphologic response units: evaluation against field data. Hydrol. Earth Syst. Sci. 17, 2981–3004.
Viseur, S., 2013. Facies and fracture detection using multiple-point statistics. 33rd GOCAD Meeting, Nancy, p. 6.
Visser, H., de Nijs, T., 2006. The Map Comparison Kit. Environ. Model. Softw. 21, 346–358.
Williams, M., Kuhn, W., Painho, M., 2012. The influence of landscape variation on landform categorization. J. Spat. Inf. Sci. 5, 51–73.
Wojcik, R., McLaughlin, D., Konings, A.G., Entekhabi, D., 2009. Conditioning stochastic rainfall replicates on remote sensing data. IEEE Trans. Geosci. Remote Sens. 47, 2436–2449.
Wood, J.D., 1996. The Geomorphological Characterisation of Digital Elevation Models. Ph. D. thesis University of Leicester, UK.
Wu, J., 2007. 4D Seismic and Multiple-point Pattern Data Integration Using Geostatistics. Ph.D. thesis Stanford University, USA.
Zevenbergen, L.W., Thorne, C.R., 1987. Quantitative analysis of land surface topography. Earth Surf. Process. Landforms 12, 47–56.
Zhang, T., Switzer, P., Journel, A., 2006. Filter-based classification of training image patterns for spatial simulation. Math. Geol. 38, 63–80.